Maximum-principle-preserving and positivity-preserving central WENO schemes on overlapping meshes

Zhanjing Tao * Zhengfu Xu † Jianxian Qiu ‡

Abstract

In this paper, we propose a class of maximum-principle-preserving central WENO schemes for scalar conservation laws, and positivity-preserving central WENO schemes for compressible Euler equations. Formulated in a finite volume framework on overlapping meshes, the central schemes require neither flux splitting nor numerical fluxes that are often exact or approximate Riemann solvers. A new fifth-order WENO reconstruction is applied for the spatial discretization, and the linear weights of such reconstruction can be any positive number as long as their sum equals one, which leads to much simpler implementation. The sufficient conditions are provided for the cell average values to preserve maximum principle or positivity property with Euler forward time discretization. The method can be generalized to high-order strong stability preserving Runge-Kutta method without technical difficulties. Extensive numerical examples are presented to illustrate the accuracy and performance of the proposed methods.

Keywords: Maximum-principle-preserving; positivity-preserving; central scheme; WENO reconstruction; overlapping mesh.

*School of Mathematics, Jilin University, Changchun, Jilin 130012, People's Republic of China. zjtao@jlu.edu.cn. Research is supported by NSFC grant 12001231.

†Department of Mathematical Science, Michigan Technological University, Houghton, MI 49931 U.S.A. zhengfux@mtu.edu.

‡School of Mathematical Sciences and Fujian Provincial Key Laboratory of Mathematical Modeling and High-Performance Scientific Computing, Xiamen University, Xiamen, Fujian 361005, People's Republic of China. jxqiu@xmu.edu.cn. Research is supported by NSFC grant 12071392.

1 Introduction

In this paper, we are interested in the initial problem for hyperbolic conservation laws

$$\begin{cases} u_t + \nabla \cdot f(u) = 0, \\ u(\mathbf{x}, 0) = u_0(\mathbf{x}). \end{cases} \tag{1}$$

Here equation (1) can be scalar or a system, and it is often nonlinear. The solution to the scalar conservation law has a maximum-principle-preserving (MPP) property such that, if the initial value is bounded $m \leq u(\mathbf{x}, 0) \leq M$, then the solution is also bounded $m \leq u(\mathbf{x}, t) \leq M$ for $t > 0$. Similarly, the solutions to the compressible Euler system have a positivity-preserving (PP) property such that both density and pressure should keep positive in every situation.

Solutions outside of $[m, M]$ might be meaningless, such as probability distribution larger than one or negative percentage. Furthermore, negative density or pressure in gas dynamics equations may lead to instability of system, and this explains that the failure of preserving the positivity of density or pressure may cause blow-ups in the numerical simulations. The E-schemes such as Godunov, Lax-Friedrichs as well as Engquist-Osher methods are total-variation-diminishing (TVD) and thus MPP. However, any TVD scheme is at most first-order around smooth extrema. The first- and second-order positivity-preserving schemes were designed in [6, 13]. For the successful high-order methods, such as Runge-Kutta discontinuous Galerkin (RKDG) and weighted essentially non-oscillatory (WENO) schemes, many efforts have been made to satisfy MPP or PP properties for the robustness and the physical relevance of the numerical solutions. In [23], Zhang and Shu proposed MPP finite volume WENO and DG schemes for scalar conservation laws. A scaling limiter was constructed and applied to the reconstructed polynomials without destroying the local conservation and accuracy. This technique was further extended to preserve the positivity of density and pressure for compressible Euler equations [24, 25, 26]. In [20], Wang et al. proposed a simple and robust strategy for the PP DG schemes, and this strategy is also adopted in our paper. To improve the compactness of the stencil of spatial reconstruction, the PP Hermite WENO

(HWENO) schemes were designed in [2, 7]. Different from the above procedure, Xu developed a parametrized MPP technique by limiting the high-order numerical fluxes toward first-order monotone fluxes in a conservative scheme in the framework of Flux Corrected Transport method [22]. Later, the flux limiter was further generalized to PP finite difference and finite volume WENO schemes for compressible Euler equations [5, 21].

Compared to upwind type schemes, central schemes are a family of efficient methods for hyperbolic conservation laws. Central methods require neither flux splitting nor numerical fluxes that are often exact or approximate Riemann solvers. In 1990, Nessyahu and Tadmor first proposed a second-order central scheme [16]. With the success of [16], various high-order versions of central schemes were explored, such as central WENO or HWENO methods [8, 10, 17, 18, 19] and central DG methods [15]. In addition, MPP or PP central DG methods were developed to solve hyperbolic conservation laws [12], ideal MHD equations [4] and shallow water equations [11].

Generally, there are two interlacing meshes in the central scheme framework: primal and dual meshes. The scheme defined on staggered mesh evolves only one set of the numerical solution at each discrete time level, and the solution is updated in a staggered fashion. The scheme using overlapping mesh evolves two sets of the numerical solution at each discrete time level. An immediate advantage of the overlapping mesh is that the SSP RungeKutta time discretizations can be applied easily.

In this paper, we construct a class of MPP and PP central WENO schemes on overlapping meshes for scalar conservation laws and compressible Euler equations, respectively. The sufficient conditions for the cell averages to preserve MPP or PP property are first provided with the Euler forward time discretization. Since the high-order strong stability preserving (SSP) Runge-Kutta method is a convex combination of Euler forward, the schemes with high-order SSP Runge-Kutta method will still maintain MPP or PP properties. This motivates us to use overlapping meshes instead of staggered meshes due to the fact that a SSP Runge-Kutta method can not be applied to staggered meshes directly. Different from the

central schemes on overlapping meshes developed in [14], a high-order WENO-AO reconstruction [1] is employed in our scheme, and the linear weights of such reconstruction can be any convex combination. For the MPP finite volume WENO scheme in [23], one needs to construct the approximation polynomials after the WENO reconstructions of point values. Alternatively, a simplified implementation of the MPP and PP limiters is proposed in [25], and one can achieve the same bound preserving property without the construction for the explicit polynomials. This technique is also used in our schemes which leads to better cost efficiency.

The paper is organized as follows. In Section 2, we introduce the central schemes on overlapping meshes with the fifth-order WENO reconstruction [1]. Then, we describe the MPP central WENO schemes for one- and two-dimensional scalar conservation laws in Section 3. In Section 4, we discuss the PP central WENO schemes for one- and two-dimensional compressible Euler equations. In Section 5, extensive numerical experiments are provided to demonstrate the performance of the proposed methods for some demanding examples in one and two dimensions. Concluding remarks are made in Section 6.

2 Central WENO schemes on overlapping meshes

2.1 One-dimensional case

We consider scalar conservation law in one dimension

$$\begin{cases} u_t + f(u)_x = 0, \\ u(x,0) = u_0(x). \end{cases} \tag{2}$$

The proposed method will be defined on overlapping meshes and evolves two copies of numerical solutions. For simplicity, the uniform mesh size Δx is used. We denote the cell of the *primal* and *dual* mesh as $I_i = [x_{i-1/2},\, x_{i+1/2}]$ and $I_{i+1/2} = [x_i,\, x_{i+1}]$, respectively. The cell centers of I_i and $I_{i+1/2}$ are $x_i = \frac{1}{2}(x_{i-1/2} + x_{i+1/2})$ and $x_{i+1/2} = \frac{1}{2}(x_i + x_{i+1})$.

We assume there exists polynomials $u_h^{n,C}(x)$ and $u_h^{n,D}(x)$ over cells I_i and $I_{i+1/2}$, respec-

tively, at $t = t_n$, and the cell averages are available

$$\overline{u}_i^{n,C} = \frac{1}{\Delta x}\int_{I_i} u_h^{n,C}(x)dx, \quad \overline{u}_{i+1/2}^{n,D} = \frac{1}{\Delta x}\int_{I_{i+1/2}} u_h^{n,D}(x)dx.$$

The central scheme on overlapping meshes [14] is applied to evaluate the solutions at $t^{n+1} = t^n + \Delta t_n$ with the Euler forward in time

$$\overline{u}_i^{n+1,C} = \theta\frac{1}{\Delta x}\int_{I_i} u_h^{n,D}(x)dx + (1-\theta)\overline{u}_i^{n,C} - \frac{\Delta t_n}{\Delta x}\left[f(u_h^{n,D}(x_{i+1/2})) - f(u_h^{n,D}(x_{i-1/2}))\right], \quad (3)$$

$$\overline{u}_{i+1/2}^{n+1,D} = \theta\frac{1}{\Delta x}\int_{I_{i+1/2}} u_h^{n,C}(x)dx + (1-\theta)\overline{u}_{i+1/2}^{n,D} - \frac{\Delta t_n}{\Delta x}\left[f(u_h^{n,C}(x_{i+1})) - f(u_h^{n,C}(x_i))\right], \quad (4)$$

where $\theta = \frac{\Delta t_n}{\tau_n}$ with τ_n being the maximal time step allowed by the CFL restriction at t_n. The semi-discrete scheme can be obtained by moving $\overline{u}_i^{n,C}$ and $\overline{u}_{i+1/2}^{n,D}$ to the left-hand side and dividing both sides by Δt_n, then passing the limit as $\Delta t_n \to 0$,

$$\frac{d}{dt}\overline{u}_i^C(t_n) = \frac{1}{\tau_n}\left(\frac{1}{\Delta x}\int_{I_i} u_h^{n,D}(x)dx - \overline{u}_i^{n,C}\right) - \frac{1}{\Delta x}\left[f(u_h^{n,D}(x_{i+1/2})) - f(u_h^{n,D}(x_{i-1/2}))\right], \quad (5)$$

$$\frac{d}{dt}\overline{u}_{i+1/2}^D(t_n) = \frac{1}{\tau_n}\left(\frac{1}{\Delta x}\int_{I_{i+1/2}} u_h^{n,C}(x)dx - \overline{u}_{i+1/2}^{n,D}\right) - \frac{1}{\Delta x}\left[f(u_h^{n,C}(x_{i+1})) - f(u_h^{n,C}(x_i))\right]. \quad (6)$$

In the scheme (3), it is useful to notice that

$$\frac{1}{\Delta x}\int_{I_i} u_h^{n,D}(x)dx = \frac{1}{\Delta x}\int_{x_{i-1/2}}^{x_i} u_h^{n,D}(x)dx + \frac{1}{\Delta x}\int_{x_i}^{x_{i+1/2}} u_h^{n,D}(x)dx.$$

This implies that one would want to get the half-cell averages $\frac{1}{\Delta x}\int_{x_{i-1/2}}^{x_i} u_h^{n,D}(x)dx$ and $\frac{1}{\Delta x}\int_{x_i}^{x_{i+1/2}} u_h^{n,D}(x)dx$. This is likewise for $\frac{1}{\Delta x}\int_{I_{i+1/2}} u_h^{n,C}(x)dx$.

2.1.1 A fifth-order WENO reconstruction

For the brevity of presentation, we only describe the WENO reconstruction for $u_h^{n,C}(x)$, and that for $u_h^{n,D}(x)$ is similar. Here, the fifth-order WENO-AO reconstruction by Balsara et al. is adopted. In Section 5, We compare the performance of the fifth-order WENO-AO, WENO-MR [28] and WENO-ZQ [27] reconstructions for the 2D Sedov problem in the example 5.8, and find that the WENO-AO reconstruction outperforms the other two reconstructions. We first introduce three small stencils $S_1 = \{I_{i-2}, I_{i-1}, I_i\}$, $S_2 = \{I_{i-1}, I_i, I_{i+1}\}$,

$S_3 = \{I_i, I_{i+1}, I_{i+2}\}$, one large stencil $\mathcal{T} = \{S_1, S_2, S_3\}$, and reconstruct one quartic polynomial $p_0(x)$ on $\mathcal{T}$, and three quadratic polynomials $p_1(x), p_2(x), p_3(x)$ on S_1, S_2, S_3, respectively, satisfying the following conditions,

$$\begin{aligned}
&\frac{1}{\Delta x}\int_{I_{i+j}} p_0(x)dx = \overline{u}_{i+j}, \quad j = -2,-1,0,1,2,\\
&\frac{1}{\Delta x}\int_{I_{i+j}} p_1(x)dx = \overline{u}_{i+j}, \quad j = -2,-1,0,\\
&\frac{1}{\Delta x}\int_{I_{i+j}} p_2(x)dx = \overline{u}_{i+j}, \quad j = -1,0,1,\\
&\frac{1}{\Delta x}\int_{I_{i+j}} p_3(x)dx = \overline{u}_{i+j}, \quad j = 0,1,2.
\end{aligned} \tag{7}$$

We have the following linear relation

$$p_0(x) = \gamma_0\left(\frac{1}{\gamma_0}p_0(x) - \frac{\gamma_1}{\gamma_0}p_1(x) - \frac{\gamma_2}{\gamma_0}p_2(x) - \frac{\gamma_3}{\gamma_0}p_3(x)\right) + \gamma_1 p_1(x) + \gamma_2 p_2(x) + \gamma_3 p_3(x).$$

By introducing two positive parameters γ_{Hi} and γ_{Lo}, both of which are always less than unity, the linear weights γ_j, $j = 0,1,2,3$ can be defined by

$$\gamma_0 = \gamma_{Hi},\ \gamma_1 = \gamma_3 = \frac{(1-\gamma_{Hi})(1-\gamma_{Lo})}{2},\ \gamma_2 = (1-\gamma_{Hi})\gamma_{Lo}.$$

Notice that $\gamma_1 + \gamma_2 + \gamma_3 = 1 - \gamma_{Hi}$, and S_2 is the central stencil among the stencils S_1, S_2, S_3. To preserve a linear stability in smooth region, we would need to assign larger linear weights to stencil S_2 than to the other two stencils. In our paper, we set $\gamma_{Hi} = 0.3$ and $\gamma_{Lo} = 0.85$. In addition, the smoothness indicators $\beta_j, j = 0,1,2,3$ are computed as below

$$\beta_j = \sum_{l=1}^{r}\int_{I_i} \Delta x^{2l-1}\left(\frac{\partial^l}{\partial x^l}p_j(x)\right)^2 dx.$$

where r is the degree of the reconstructed polynomials $p_j(x), j = 0,1,2,3$.

With the linear weights and smoothness indicators, we now describe the process of computing the nonlinear weights. There are two approaches to obtain the nonlinear weights in [1]. The first approach is given by

$$\tau = \frac{1}{3}\left(|\beta_0 - \beta_1| + |\beta_0 - \beta_2| + |\beta_0 - \beta_3|\right)$$

$$\omega_j = \frac{\overline{\omega}_j}{\sum_{k=0}^{3} \overline{\omega}_k},\ j = 0, 1, 2, 3, \quad \text{where } \overline{\omega}_k = \gamma_k \left(1 + \frac{\tau^2}{(\varepsilon + \beta_k)^2}\right),\ k = 0, 1, 2, 3, \tag{8}$$

while the second one is

$$\omega_j = \frac{\overline{\omega}_j}{\sum_{k=0}^{3} \overline{\omega}_k},\ j = 0, 1, 2, 3, \quad \text{where } \overline{\omega}_k = \frac{\gamma_k}{(\varepsilon + \beta_k)^2},\ k = 0, 1, 2, 3. \tag{9}$$

Here $\varepsilon > 0$ is a small constant to avoid the denominator to be zero and we use $\varepsilon = 10^{-6}$ for the numerical examples, unless otherwise stated. The authors [1] demonstrated that equation (9) is a more stable option, while equation (8) is more accurate, and we use equation (9) in this paper.

Finally, we want to obtain a nonlinear hybridization between the fifth-order polynomial $p_0(x)$ and the three third-order polynomials $p_1(x), p_2(x), p_3(x)$. Such a combination strategy was developed in earlier references [3, 9, 27], and the final fifth-order reconstructed polynomial is given as

$$P(x) = \omega_0 \left(\frac{1}{\gamma_0} p_0(x) - \frac{\gamma_1}{\gamma_0} p_1(x) - \frac{\gamma_2}{\gamma_0} p_2(x) - \frac{\gamma_3}{\gamma_0} p_3(x)\right) + \omega_1 p_1(x) + \omega_2 p_2(x) + \omega_3 p_3(x).$$

The cell averages and point values in the scheme (4) can be approximated by the reconstructed polynomial $P(x)$.

2.2 Two-dimensional case

We consider scalar conservation law in two dimensions

$$\begin{cases} u_t + f(u)_x + g(u)_y = 0, \\ u(x, y, 0) = u_0(x, y). \end{cases} \tag{10}$$

The proposed numerical method will be defined on overlapping meshes and evolves two copies of numerical solutions. The uniform mesh sizes Δx in the x direction, and Δy in the y direction are used. We denote the cell of the *primal* and *dual* mesh as $I_{ij} = [x_{i-1/2}, x_{i+1/2}] \times [y_{j-1/2}, y_{j+1/2}]$ and $I_{i+1/2,j+1/2} = [x_i, x_{i+1}] \times [y_j, y_{j+1}]$, respectively. The cell centers of I_{ij} and $I_{i+1/2,j+1/2}$ are (x_i, y_j) and $(x_{i+1/2}, y_{j+1/2})$.

We assume there exists polynomials $u_h^{n,C}(x,y)$ and $u_h^{n,D}(x,y)$ over cells I_{ij} and $I_{i+1/2,j+1/2}$, respectively, at $t=t_n$, and the cell averages are available

$$\overline{u}_{ij}^{n,C}=\frac{1}{\Delta x\Delta y}\int_{I_{ij}}u_h^{n,C}(x,y)dxdy,\quad \overline{u}_{i+1/2,j+1/2}^{n,D}=\frac{1}{\Delta x\Delta y}\int_{I_{i+1/2,j+1/2}}u_h^{n,D}(x,y)dxdy.$$

To obtain the numerical solution $\overline{u}_{ij}^{n+1,C}$ and $\overline{u}_{i+1/2,j+1/2}^{n+1,D}$ at $t=t_{n+1}$, we apply the central scheme on overlapping meshes with Euler forward time discretization to (10)

$$\begin{aligned}\overline{u}_{ij}^{n+1,C}=&\theta\frac{1}{\Delta x\Delta y}\int_{I_{ij}}u_h^{n,D}(x,y)dxdy+(1-\theta)\overline{u}_{ij}^{n,C}\\&-\frac{\Delta t_n}{\Delta x\Delta y}\int_{y_{j-1/2}}^{y_{j+1/2}}\left[f(u_h^{n,D}(x_{i+1/2},y))-f(u_h^{n,D}(x_{i-1/2},y))\right]dy\\&-\frac{\Delta t_n}{\Delta x\Delta y}\int_{x_{i-1/2}}^{x_{i+1/2}}\left[g(u_h^{n,D}(x,y_{j+1/2}))-g(u_h^{n,D}(x,y_{j-1/2}))\right]dx,\end{aligned}\tag{11}$$

$$\begin{aligned}\overline{u}_{i+1/2,j+1/2}^{n+1,D}=&\theta\frac{1}{\Delta x\Delta y}\int_{I_{i+1/2,j+1/2}}u_h^{n,C}(x,y)dxdy+(1-\theta)\overline{u}_{i+1/2,j+1/2}^{n,D}\\&-\frac{\Delta t_n}{\Delta x\Delta y}\int_{y_j}^{y_{j+1}}\left[f(u_h^{n,C}(x_{i+1},y))-f(u_h^{n,C}(x_i,y))\right]dy\\&-\frac{\Delta t_n}{\Delta x\Delta y}\int_{x_i}^{x_{i+1}}\left[g(u_h^{n,C}(x,y_{j+1}))-g(u_h^{n,C}(x,y_j))\right]dx,\end{aligned}\tag{12}$$

where $\theta=\frac{\Delta t_n}{\tau_n}$ with τ_n being the maximal time step allowed by the CFL restriction at t_n. The semi-discrete scheme can be obtained by moving $\overline{u}_{ij}^{n,C}$ and $\overline{u}_{i+1/2,j+1/2}^{n,D}$ to the left-hand side and dividing both sides by Δt_n, then passing the limit as $\Delta t_n\to 0$,

$$\begin{aligned}\frac{d}{dt}\overline{u}_{ij}^{C}(t_n)=&\frac{1}{\tau_n}\left(\frac{1}{\Delta x\Delta y}\int_{I_{ij}}u_h^{n,D}(x,y)dxdy-\overline{u}_{ij}^{n,C}\right)\\&-\frac{1}{\Delta x\Delta y}\int_{y_{j-1/2}}^{y_{j+1/2}}\left[f(u_h^{n,D}(x_{i+1/2},y))-f(u_h^{n,D}(x_{i-1/2},y))\right]dy\\&-\frac{1}{\Delta x\Delta y}\int_{x_{i-1/2}}^{x_{i+1/2}}\left[g(u_h^{n,D}(x,y_{j+1/2}))-g(u_h^{n,D}(x,y_{j-1/2}))\right]dx,\end{aligned}\tag{13}$$

$$\begin{aligned}\frac{d}{dt}\overline{u}_{i+1/2,j+1/2}^{D}(t_n)=&\frac{1}{\tau_n}\left(\frac{1}{\Delta x\Delta y}\int_{I_{i+1/2,j+1/2}}u_h^{n,C}(x,y)dxdy-\overline{u}_{i+1/2,j+1/2}^{n,D}\right)\\&-\frac{1}{\Delta x\Delta y}\int_{y_j}^{y_{j+1}}\left[f(u_h^{n,C}(x_{i+1},y))-f(u_h^{n,C}(x_i,y))\right]dy\\&-\frac{1}{\Delta x\Delta y}\int_{x_i}^{x_{i+1}}\left[g(u_h^{n,C}(x,y_{j+1}))-g(u_h^{n,C}(x,y_j))\right]dx.\end{aligned}\tag{14}$$

In the same spirit as in one dimension, one would want to get the following four quarter-cell averages to obtain the cell average $\frac{1}{\Delta x\Delta y}\int_{I_{ij}} u_h^{n,D}(x,y)dxdy$,

$$\begin{aligned}
&\frac{1}{\Delta x\Delta y}\int_{x_{i-1/2}}^{x_i}\int_{y_{j-1/2}}^{y_j} u_h^{n,D}(x,y)dxdy, \quad \frac{1}{\Delta x\Delta y}\int_{x_i}^{x_{i+1/2}}\int_{y_{j-1/2}}^{y_j} u_h^{n,D}(x,y)dxdy,\\
&\frac{1}{\Delta x\Delta y}\int_{x_{i-1/2}}^{x_i}\int_{y_j}^{y_{j+1/2}} u_h^{n,D}(x,y)dxdy, \quad \frac{1}{\Delta x\Delta y}\int_{x_i}^{x_{i+1/2}}\int_{y_j}^{y_{j+1/2}} u_h^{n,D}(x,y)dxdy.
\end{aligned} \tag{15}$$

This similarly goes to $\frac{1}{\Delta x\Delta y}\int_{I_{i+1/2,j+1/2}} u_h^{n,C}(x,y)dxdy$. In addition, the appropriate Gaussian quadrature is used to compute the integrals of flux in (11)-(12).

2.2.1 Reconstruction procedure

Based on one-dimensional WENO reconstruction in Section 2.1.1, the dimension-by-dimension approach is applied to get the cell averages and point values in the schemes (11)-(12).

2.3 High-order time discretization

Since Euler forward time discretization is only first-order, we will use a high-order SSP time discretization. In our implementations, the third-order SSP Runge-Kutta method is exploited

$$\begin{aligned}
u^{(1)} &= u^n + \Delta t L(u^n),\\
u^{(2)} &= \frac{3}{4}u^n + \frac{1}{4}\left(u^{(1)} + \Delta t L(u^{(1)})\right),\\
u^{n+1} &= \frac{1}{3}u^n + \frac{2}{3}\left(u^{(2)} + \Delta t L(u^{(2)})\right).
\end{aligned} \tag{16}$$

where $L(u)$ is the spatial operator. Note that a high-order SSP time discretization is a convex combination of Euler forward.

3 Maximum-principle-preserving central WENO schemes for scalar conservation laws

In general, the schemes (3)-(4) and (11)-(12) do not satisfy the maximum principle and we want to design MPP central WENO schemes. Here, we only focus on the procedure to

update $\overline{u}_i^{n+1,C}$ and $\overline{u}_{ij}^{n+1,C}$ in one- and two-dimensional case, respectively, and this similarly goes to $\overline{u}_{i+1/2}^{n+1,D}$ and $\overline{u}_{i+1/2,j+1/2}^{n+1,D}$.

3.1 One-dimensional case

For the ease of presentation, we assume that there is a reconstructed polynomial $u_h^{n,D}(x)$ over the cell $I_{i+1/2}$ with cell average $\overline{u}_{i+1/2}^{n,D}$. Then, the left and right half-cell averages of $u_h^{n,D}(x)$ over the cell $I_{i+1/2}$ are defined as follows,

$$\overline{u}_{i+1/2}^{l} = \frac{1}{\Delta x}\int_{x_i}^{x_{i+1/2}} u_h^{n,D}(x)dx, \quad \overline{u}_{i+1/2}^{r} = \frac{1}{\Delta x}\int_{x_{i+1/2}}^{x_{i+1}} u_h^{n,D}(x)dx = \overline{u}_{i+1/2}^{n,D} - \overline{u}_{i+1/2}^{l}.$$

Since our scheme is fifth-order, we consider the four point Gauss-Lobatto quadrature, which is exact for integral of polynomial $u_h^{n,D}(x)$. The half-cell averages can be evaluated as below

$$\overline{u}_{i+1/2}^{l} = \sum_{\alpha=1}^{3}\frac{\hat{\omega}_\alpha}{2}u_h^{n,D}(\hat{x}_{i+1/2}^{\alpha,l}) + \frac{\hat{\omega}_4}{2}u_h^{n,D}(\hat{x}_{i+1/2}^{4,l}) = \sum_{\alpha=1}^{3}\frac{\hat{\omega}_\alpha}{2}u_h^{n,D}(\hat{x}_{i+1/2}^{\alpha,l}) + \frac{\hat{\omega}_4}{2}u_h^{n,D}(x_{i+1/2}),$$

$$\overline{u}_{i+1/2}^{r} = \frac{\hat{\omega}_1}{2}u_h^{n,D}(\hat{x}_{i+1/2}^{1,r}) + \sum_{\alpha=2}^{4}\frac{\hat{\omega}_\alpha}{2}u_h^{n,D}(\hat{x}_{i+1/2}^{\alpha,r}) = \frac{\hat{\omega}_1}{2}u_h^{n,D}(x_{i+1/2}) + \sum_{\alpha=2}^{4}\frac{\hat{\omega}_\alpha}{2}u_h^{n,D}(\hat{x}_{i+1/2}^{\alpha,r}),$$

where $\hat{x}_{i+1/2}^{\alpha,l}$ and $\hat{x}_{i+1/2}^{\alpha,r}$ are Gauss-Lobatto quadrature points in the interval $[x_i, x_{i+1/2}]$ and $[x_{i+1/2}, x_{i+1}]$, respectively, and $\hat{\omega}_\alpha\,(\alpha = 1, \cdots, 4)$ are corresponding quadrature weights on the interval $[-\frac{1}{2}, \frac{1}{2}]$. Note that $\hat{x}_{i+1/2}^{4,l} = \hat{x}_{i+1/2}^{1,r} = x_{i+1/2}$.

Based on the simplified implementation of the MPP limiter in [25] and mean value theorem, there exists $\xi_{i+1/2}^{l} \in [x_i, x_{i+1/2}]$ and $\xi_{i+1/2}^{r} \in [x_{i+1/2}, x_{i+1}]$, such that

$$u_h^{n,D}(\xi_{i+1/2}^{l}) = \frac{1}{1-\hat{\omega}_4}\sum_{\alpha=1}^{3}\hat{\omega}_\alpha u_h^{n,D}(\hat{x}_{i+1/2}^{\alpha,l}) = \frac{1}{1-\hat{\omega}_4}\left(2\overline{u}_{i+1/2}^{l} - \hat{\omega}_4 u_h^{n,D}(x_{i+1/2})\right) \tag{17}$$

$$u_h^{n,D}(\xi_{i+1/2}^{r}) = \frac{1}{1-\hat{\omega}_1}\sum_{\alpha=2}^{4}\hat{\omega}_\alpha u_h^{n,D}(\hat{x}_{i+1/2}^{\alpha,r}) = \frac{1}{1-\hat{\omega}_1}\left(2\overline{u}_{i+1/2}^{r} - \hat{\omega}_1 u_h^{n,D}(x_{i+1/2})\right) \tag{18}$$

Then, the half-cell averages can be written as

$$\overline{u}_{i+1/2}^{l} = \frac{1-\hat{\omega}_4}{2}u_h^{n,D}(\xi_{i+1/2}^{l}) + \frac{\hat{\omega}_4}{2}u_h^{n,D}(x_{i+1/2}), \tag{19}$$

$$\overline{u}_{i+1/2}^{r} = \frac{\hat{\omega}_1}{2}u_h^{n,D}(x_{i+1/2}) + \frac{1-\hat{\omega}_1}{2}u_h^{n,D}(\xi_{i+1/2}^{r}). \tag{20}$$

Plug (19)-(20) into the scheme (3), we obtain

$$\begin{aligned}
\overline{u}_i^{n+1,C} =&(1-\theta)\overline{u}_i^{n,C} + \theta\frac{1}{\Delta x}\int_{I_i} u_h^{n,D}(x)dx - \lambda\left(f(u_h^{n,D}(x_{i+1/2})) - f(u_h^{n,D}(x_{i-1/2}))\right)\\
=&(1-\theta)\overline{u}_i^{n,C} + \theta\frac{1}{\Delta x}\left(\int_{x_{i-1/2}}^{x_i} u_h^{n,D}(x)dx + \int_{x_i}^{x_{i+1/2}} u_h^{n,D}(x)dx\right)\\
&-\lambda\left(f(u_h^{n,D}(x_{i+1/2})) - f(u_h^{n,D}(x_{i-1/2}))\right)\\
=&(1-\theta)\overline{u}_i^{n,C} + \left(\frac{\theta}{2}(1-\hat{\omega}_1)u_h^{n,D}(\xi_{i-1/2}^r) + \frac{\theta}{2}\hat{\omega}_1 u_h^{n,D}(x_{i-1/2}) + \lambda f(u_h^{n,D}(x_{i-1/2}))\right)\\
&+\left(\frac{\theta}{2}(1-\hat{\omega}_4)u_h^{n,D}(\xi_{i+1/2}^l) + \frac{\theta}{2}\hat{\omega}_4 u_h^{n,D}(x_{i+1/2}) - \lambda f(u_h^{n,D}(x_{i+1/2}))\right)\\
=&(1-\theta)\overline{u}_i^{n,C} + \frac{\theta}{2}\left((1-\hat{\omega}_1)u_h^{n,D}(\xi_{i-1/2}^r) + (1-\hat{\omega}_4)u_h^{n,D}(\xi_{i+1/2}^l)\right)\\
&+\left(\frac{\theta}{2}\hat{\omega}_1 u_h^{n,D}(x_{i-1/2}) + \lambda f(u_h^{n,D}(x_{i-1/2}))\right) + \left(\frac{\theta}{2}\hat{\omega}_4 u_h^{n,D}(x_{i+1/2}) - \lambda f(u_h^{n,D}(x_{i+1/2}))\right)
\end{aligned} \tag{21}$$

where $\lambda = \frac{\Delta t_n}{\Delta x}$. Following the idea of Theorem 2.1 in [12], we have

Theorem 3.1. For the scheme (21), assume $\overline{u}_i^{n,C}, \overline{u}_{i+1/2}^{n,D} \in [m, M]$, $\forall i$. If the values $u_h^{n,D}(\xi_{i+1/2}^l)$, $u_h^{n,D}(\xi_{i+1/2}^r)$ and $u_h^{n,D}(x_{i+1/2})$, $\forall i$, are in the range $[m, M]$, then $\overline{u}_i^{n+1,C} \in [m, M]$, $\forall i$, under the CFL condition

$$\lambda a \leqslant \frac{\theta}{2}\hat{\omega}_1. \tag{22}$$

where $a = \max\left(||f'(u_h^{n,C}(\cdot))||_\infty, ||f'(u_h^{n,D}(\cdot))||_\infty\right)$.

Proof. Notice that

$$\begin{aligned}
\overline{u}_i^{n+1,C} =&(1-\theta)\overline{u}_i^{n,C} + \frac{\theta}{2}\left((1-\hat{\omega}_1)u_h^{n,D}(\xi_{i-1/2}^r) + (1-\hat{\omega}_4)u_h^{n,D}(\xi_{i+1/2}^l)\right)\\
&+\left(\frac{\theta}{2}\hat{\omega}_1 u_h^{n,D}(x_{i-1/2}) + \lambda f(u_h^{n,D}(x_{i-1/2}))\right) + \left(\frac{\theta}{2}\hat{\omega}_4 u_h^{n,D}(x_{i+1/2}) - \lambda f(u_h^{n,D}(x_{i+1/2}))\right)\\
=&: H(\overline{u}_i^{n,C}, u_h^{n,D}(\xi_{i-1/2}^r), u_h^{n,D}(\xi_{i+1/2}^l), u_h^{n,D}(x_{i-1/2}), u_h^{n,D}(x_{i+1/2}).
\end{aligned}$$

Since $\hat{\omega}_1 = \hat{\omega}_4$, we clearly have

$$\begin{aligned}
\frac{\partial H}{\partial \overline{u}_i^{n,C}} &= 1-\theta \geq 0 \\
\frac{\partial H}{\partial u_h^{n,D}(\xi_{i-1/2}^r)} &= \frac{\theta}{2}(1-\hat{\omega}_1) \geq 0 \\
\frac{\partial H}{\partial u_h^{n,D}(\xi_{i+1/2}^l)} &= \frac{\theta}{2}(1-\hat{\omega}_4) \geq 0 \\
\frac{\partial H}{\partial u_h^{n,D}(x_{i-1/2})} &= \frac{\theta}{2}\hat{\omega}_1\left(1+\frac{\lambda}{\frac{\theta}{2}\hat{\omega}_1}f'(u_h^{n,D}(x_{i-1/2}))\right) \geq \frac{\theta}{2}\hat{\omega}_1\left(1-\frac{\lambda a}{\frac{\theta}{2}\hat{\omega}_1}\right) \geq 0 \\
\frac{\partial H}{\partial u_h^{n,D}(x_{i+1/2})} &= \frac{\theta}{2}\hat{\omega}_4\left(1-\frac{\lambda}{\frac{\theta}{2}\hat{\omega}_4}f'(u_h^{n,D}(x_{i+1/2}))\right) \geq \frac{\theta}{2}\hat{\omega}_4\left(1-\frac{\lambda a}{\frac{\theta}{2}\hat{\omega}_4}\right) \geq 0
\end{aligned}$$

Due to the consistency of the scheme, we have

$$m = H(m,m,m,m,m) \leq \overline{u}_i^{n+1,C} \leq H(M,M,M,M,M) = M.$$

□

Given $\overline{u}_i^{n,C}, \overline{u}_{i+1/2}^{n,D} \in [m,M]$, the algorithm to update $\overline{u}_i^{n+1,C}$ in the MPP central WENO scheme with Euler forward time discretization is:

1. Evaluate the half-cell averages $\frac{1}{\Delta x}\int_{x_i}^{x_{i+1/2}} u_h^{n,D}(x)dx$, $\frac{1}{\Delta x}\int_{x_{i+1/2}}^{x_{i+1}} u_h^{n,D}(x)dx$, and the point values $u_h^{n,D}(x_{i+1/2})$ in the cell $I_{i+1/2}$ based on the WENO reconstruction.

2. Compute $u_h^{n,D}(\xi_{i+1/2}^l)$ and $u_h^{n,D}(\xi_{i+1/2}^r)$ by (17) - (18).

3. Modify the point values by the following MPP scaling limiter

$$\alpha = \min\left\{1, \left|\frac{M-\overline{u}_{i+1/2}^{n,D}}{M_{i+1/2}-\overline{u}_{i+1/2}^{n,D}}\right|, \left|\frac{m-\overline{u}_{i+1/2}^{n,D}}{m_{i+1/2}-\overline{u}_{i+1/2}^{n,D}}\right|\right\},$$

$$\widetilde{u}_h^{n,D}(x) = \alpha\left(u_h^{n,D}(x)-\overline{u}_{i+1/2}^{n,D}\right)+\overline{u}_{i+1/2}^{n,D}, \quad x \in S_{i+1/2},$$

with

$$M_{i+1/2} = \max_{x\in S_{i+1/2}} u_h^{n,D}(x), \quad m_{i+1/2} = \min_{x\in S_{i+1/2}} u_h^{n,D}(x), \quad S_{i+1/2} = \{x_{i+1/2}, \xi_{i+1/2}^l, \xi_{i+1/2}^r\}.$$

After the limiter, we can enforce $\widetilde{u}_h^{n,D}(x) \in [m,M],\ x \in S_{i+1/2}$.

4. Use $\widetilde{u}_h^{n,D}(x)$ instead of $u_h^{n,D}(x)$ in the central scheme (21) under the CFL condition (22).

3.2 Two-dimensional case

For the ease of presentation, we assume that there exists a polynomial $u_h^{n,D}(x,y)$ in the cell $I_{i+1/2,j+1/2}$. We consider the four point Gauss-Lobatto and three point Gauss quadrature rule, which are exact for single variable polynomials of degree 5. Recall that $\hat{x}_{i+1/2}^{\alpha,l}$ and $\hat{x}_{i+1/2}^{\alpha,r}\,(\alpha = 1,\cdots,4)$ are the Gauss-Lobatto quadrature points in the interval $[x_i, x_{i+1/2}]$ and $[x_{i+1/2}, x_{i+1}]$, respectively, and let $\hat{y}_{j+1/2}^{\alpha,l}$ and $\hat{y}_{j+1/2}^{\alpha,r}\,(\alpha = 1,\cdots,4)$ be the Gauss-Lobatto quadrature points in the interval $[y_j, y_{j+1/2}]$ and $[y_{j+1/2}, y_{j+1}]$, respectively. $\hat{\omega}_\alpha$ are corresponding quadrature weights in the interval $[-\frac{1}{2}, \frac{1}{2}]$ such that $\sum_{\alpha=1}^{4}\hat{\omega}_\alpha = 1$. Let $x_{i+1/2}^{\beta,l}$ and $x_{i+1/2}^{\beta,r}\,(\beta = 1,2,3)$ denote Gauss quadrature points in the interval $[x_i, x_{i+1/2}]$ and $[x_{i+1/2}, x_{i+1}]$, respectively, and $y_{j+1/2}^{\beta,l}$ and $y_{j+1/2}^{\beta,r}\,(\beta = 1,2,3)$ denote Gauss quadrature points in the interval $[y_j, y_{j+1/2}]$ and $[y_{j+1/2}, y_{j+1}]$, respectively. ω_β are corresponding quadrature weights in the interval $[-\frac{1}{2}, \frac{1}{2}]$ such that $\sum_{\beta=1}^{3}\omega_\beta = 1$. In this paper, subscript or superscript α will be used only for Gauss-Lobatto quadrature and β only for Gauss quadrature.

Based on $\hat{\omega}_1 = \hat{\omega}_4$ and the mean value theorem, there exists some points

$$(\xi_{i+1/2}^1, \eta_{j+1/2}^1) \in [x_i, x_{i+1/2}] \times [y_j, y_{j+1/2}],\ (\xi_{i+1/2}^2, \eta_{j+1/2}^2) \in [x_{i+1/2}, x_{i+1}] \times [y_j, y_{j+1/2}]$$
$$(\xi_{i+1/2}^3, \eta_{j+1/2}^3) \in [x_i, x_{i+1/2}] \times [y_{j+1/2}, y_{j+1}],\ (\xi_{i+1/2}^4, \eta_{j+1/2}^4) \in [x_{i+1/2}, x_{i+1}] \times [y_{j+1/2}, y_{j+1}],$$

such that

$$u_h^{n,D}(\xi_{i+1/2}^1, \eta_{j+1/2}^1) = \frac{4W_1 - \sum_{\beta=1}^{3}\omega_\beta\hat{\omega}_1\left(\mu_1 u_h^{n,D}(x_{i+1/2}, y_{j+1/2}^{\beta,l}) + \mu_2 u_h^{n,D}(x_{i+1/2}^{\beta,l}, y_{j+1/2})\right)}{1-\hat{\omega}_1}, \tag{23}$$

$$u_h^{n,D}(\xi_{i+1/2}^2, \eta_{j+1/2}^2) = \frac{4W_2 - \sum_{\beta=1}^{3}\omega_\beta\hat{\omega}_1\left(\mu_1 u_h^{n,D}(x_{i+1/2}, y_{j+1/2}^{\beta,l}) + \mu_2 u_h^{n,D}(x_{i+1/2}^{\beta,r}, y_{j+1/2})\right)}{1-\hat{\omega}_1}, \tag{24}$$

$$u_h^{n,D}(\xi_{i+1/2}^3,\eta_{j+1/2}^3)=\frac{4W_3-\sum_{\beta=1}^3\omega_\beta\hat{\omega}_1\left(\mu_1u_h^{n,D}(x_{i+1/2},y_{j+1/2}^{\beta,r})+\mu_2u_h^{n,D}(x_{i+1/2}^{\beta,l},y_{j+1/2})\right)}{1-\hat{\omega}_1},\tag{25}$$

$$u_h^{n,D}(\xi_{i+1/2}^4,\eta_{j+1/2}^4)=\frac{4W_4-\sum_{\beta=1}^3\omega_\beta\hat{\omega}_1\left(\mu_1u_h^{n,D}(x_{i+1/2},y_{j+1/2}^{\beta,r})+\mu_2u_h^{n,D}(x_{i+1/2}^{\beta,r},y_{j+1/2})\right)}{1-\hat{\omega}_1},\tag{26}$$

where

$$W_1=\frac{1}{\Delta x\Delta y}\int_{x_i}^{x_{i+1/2}}\int_{y_j}^{y_{j+1/2}}u_h^{n,D}(x,y)dxdy,\ W_2=\frac{1}{\Delta x\Delta y}\int_{x_{i+1/2}}^{x_{i+1}}\int_{y_j}^{y_{j+1/2}}u_h^{n,D}(x,y)dxdy,$$
$$W_3=\frac{1}{\Delta x\Delta y}\int_{x_i}^{x_{i+1/2}}\int_{y_{j+1/2}}^{y_{j+1}}u_h^{n,D}(x,y)dxdy,\ W_4=\frac{1}{\Delta x\Delta y}\int_{x_{i+1/2}}^{x_{i+1}}\int_{y_{j+1/2}}^{y_{j+1}}u_h^{n,D}(x,y)dxdy,$$

and

$$\mu_1=\frac{\lambda_1a_1}{\lambda_1a_1+\lambda_2a_2},\ \mu_2=\frac{\lambda_2a_2}{\lambda_1a_1+\lambda_2a_2},\lambda_1=\frac{\Delta t_n}{\Delta x},\ \lambda_2=\frac{\Delta t_n}{\Delta y},$$
$$a_1=\max\left(||f'(u_h^{n,C}(\cdot))||_\infty,||f'(u_h^{n,D}(\cdot))||_\infty\right),a_2=\max\left(||g'(u_h^{n,C}(\cdot))||_\infty,||g'(u_h^{n,D}(\cdot))||_\infty\right).$$

For each cell $I_{i+1/2,j+1/2}$ in the dual mesh, we define

$$A=\{(\xi_{i+1/2}^1,\eta_{j+1/2}^1),(\xi_{i+1/2}^2,\eta_{j+1/2}^2),(\xi_{i+1/2}^3,\eta_{j+1/2}^3),(\xi_{i+1/2}^4,\eta_{j+1/2}^4)\},\tag{27}$$

$$L^x=\{x_{i+1/2}^{\beta,l},x_{i+1/2}^{\beta,r}:\beta=1,2,3\},\ L^y=\{y_{j+1/2}^{\beta,l},y_{j+1/2}^{\beta,r}:\beta=1,2,3\},\tag{28}$$

and

$$S_{i+1/2,j+1/2}=A\cup\{(x_{i+1/2},y):y\in L^y\}\cup\{(x,y_{j+1/2}):x\in L^x\}.\tag{29}$$

To update $\overline{u}_{ij}^{n+1,C}$ in (11), we decompose the cell average of $u_h^{n,D}(x,y)$ in the cell I_{ij} into four quarter-cell averages

$$\frac{1}{\Delta x\Delta y}\int_{I_{ij}}u_h^{n,D}(x,y)dxdy=:U_1+U_2+U_3+U_4,$$

where

$$U_1=\frac{1}{\Delta x\Delta y}\int_{x_{i-1/2}}^{x_i}\int_{y_{j-1/2}}^{y_j}u_h^{n,D}(x,y)dxdy,\quad U_2=\frac{1}{\Delta x\Delta y}\int_{x_i}^{x_{i+1/2}}\int_{y_{j-1/2}}^{y_j}u_h^{n,D}(x,y)dxdy,$$
$$U_3=\frac{1}{\Delta x\Delta y}\int_{x_{i-1/2}}^{x_i}\int_{y_j}^{y_{j+1/2}}u_h^{n,D}(x,y)dxdy,\quad U_4=\frac{1}{\Delta x\Delta y}\int_{x_i}^{x_{i+1/2}}\int_{y_j}^{y_{j+1/2}}u_h^{n,D}(x,y)dxdy.$$

Accordingly, the integral of the flux can be split as

$$\frac{1}{\Delta y}\int_{y_{j-1/2}}^{y_{j+1/2}}\left[f(u_h^{n,D}(x_{i+1/2},y))-f(u_h^{n,D}(x_{i-1/2},y))\right]dy =: F_1+F_2+F_3+F_4,$$

where

$$F_1=-\frac{1}{\Delta y}\int_{y_{j-1/2}}^{y_j} f(u_h^{n,D}(x_{i-1/2},y))dy,\quad F_2=\frac{1}{\Delta y}\int_{y_{j-1/2}}^{y_j} f(u_h^{n,D}(x_{i+1/2},y))dy,$$
$$F_3=-\frac{1}{\Delta y}\int_{y_j}^{y_{j+1/2}} f(u_h^{n,D}(x_{i-1/2},y))dy,\quad F_4=\frac{1}{\Delta y}\int_{y_j}^{y_{j+1/2}} f(u_h^{n,D}(x_{i+1/2},y))dy.$$

Similarly, we have

$$\frac{1}{\Delta x}\int_{x_{i-1/2}}^{x_{i+1/2}}\left[g(u_h^{n,D}(x,y_{j+1/2}))-g(u_h^{n,D}(x,y_{j-1/2}))\right]dx =: G_1+G_2+G_3+G_4,$$

where

$$G_1=-\frac{1}{\Delta x}\int_{x_{i-1/2}}^{x_i} g(u_h^{n,D}(x,y_{j-1/2}))dx,\quad G_2=-\frac{1}{\Delta x}\int_{x_i}^{x_{i+1/2}} g(u_h^{n,D}(x,y_{j-1/2}))dx,$$
$$G_3=\frac{1}{\Delta x}\int_{x_{i-1/2}}^{x_i} g(u_h^{n,D}(x,y_{j+1/2}))dx,\quad G_4=\frac{1}{\Delta x}\int_{x_i}^{x_{i+1/2}} g(u_h^{n,D}(x,y_{j+1/2}))dx.$$

Then, the scheme (11) becomes

$$\begin{aligned}\overline{u}_{ij}^{n+1,C} =&(1-\theta)\overline{u}_{ij}^{n,C}+\theta\left(U_1+U_2+U_3+U_4\right)\\ &-\lambda_1(F_1+F_2+F_3+F_4)-\lambda_2(G_1+G_2+G_3+G_4)\end{aligned}\tag{30}$$

Using the quadrature rule mentioned above to compute the integrals in the scheme (30), we have

$$\begin{aligned}&\theta U_1-\lambda_1F_1-\lambda_2G_1\\ =&\frac{\mu_1\theta}{\Delta x\Delta y}\int_{x_{i-1/2}}^{x_i}\int_{y_{j-1/2}}^{y_j}u_h^{n,D}(x,y)dxdy+\frac{\lambda_1}{\Delta y}\int_{y_{j-1/2}}^{y_j}f(u_h^{n,D}(x_{i-1/2},y))dy\\ &+\frac{\mu_2\theta}{\Delta x\Delta y}\int_{x_{i-1/2}}^{x_i}\int_{y_{j-1/2}}^{y_j}u_h^{n,D}(x,y)dxdy+\frac{\lambda_2}{\Delta x}\int_{x_{i-1/2}}^{x_i}g(u_h^{n,D}(x,y_{j-1/2}))dx\\ =&\frac{\mu_1\theta}{4}\sum_{\beta=1}^{3}\sum_{\alpha=1}^{4}\omega_\beta\hat{\omega}_\alpha u_h^{n,D}(\hat{x}_{i-1/2}^{\alpha,r},y_{j-1/2}^{\beta,r})+\frac{\lambda_1}{2}\sum_{\beta=1}^{3}\omega_\beta f(u_h^{n,D}(x_{i-1/2},y_{j-1/2}^{\beta,r}))\\ &+\frac{\mu_2\theta}{4}\sum_{\beta=1}^{3}\sum_{\alpha=1}^{4}\omega_\beta\hat{\omega}_\alpha u_h^{n,D}(x_{i-1/2}^{\beta,r},\hat{y}_{j-1/2}^{\alpha,r})+\frac{\lambda_2}{2}\sum_{\beta=1}^{3}\omega_\beta g(u_h^{n,D}(x_{i-1/2}^{\beta,r},y_{j-1/2}))\end{aligned}$$

$$
\begin{aligned}
=&\frac{\theta}{4}\sum_{\beta=1}^{3}\sum_{\alpha=2}^{4}\omega_\beta\hat{\omega}_\alpha\left(\mu_1 u_h^{n,D}(\hat{x}_{i-1/2}^{\alpha,r},y_{j-1/2}^{\beta,r})+\mu_2 u_h^{n,D}(x_{i-1/2}^{\beta,r},\hat{y}_{j-1/2}^{\alpha,r})\right)\\
&+\frac{\mu_1\theta}{4}\sum_{\beta=1}^{3}\omega_\beta\hat{\omega}_1 u_h^{n,D}(x_{i-1/2},y_{j-1/2}^{\beta,r})+\frac{\lambda_1}{2}\sum_{\beta=1}^{3}\omega_\beta f(u_h^{n,D}(x_{i-1/2},y_{j-1/2}^{\beta,r}))\\
&+\frac{\mu_2\theta}{4}\sum_{\beta=1}^{3}\omega_\beta\hat{\omega}_1 u_h^{n,D}(x_{i-1/2}^{\beta,r},y_{j-1/2})+\frac{\lambda_2}{2}\sum_{\beta=1}^{3}\omega_\beta g(u_h^{n,D}(x_{i-1/2}^{\beta,r},y_{j-1/2}))\\
=&\frac{\theta}{4}(1-\hat{\omega}_1)u_h^{n,D}(\xi_{i-1/2}^4,\eta_{j-1/2}^4)\\
&+\frac{\mu_1\theta}{4}\sum_{\beta=1}^{3}\omega_\beta\hat{\omega}_1 u_h^{n,D}(x_{i-1/2},y_{j-1/2}^{\beta,r})+\frac{\lambda_1}{2}\sum_{\beta=1}^{3}\omega_\beta f(u_h^{n,D}(x_{i-1/2},y_{j-1/2}^{\beta,r}))\\
&+\frac{\mu_2\theta}{4}\sum_{\beta=1}^{3}\omega_\beta\hat{\omega}_1 u_h^{n,D}(x_{i-1/2}^{\beta,r},y_{j-1/2})+\frac{\lambda_2}{2}\sum_{\beta=1}^{3}\omega_\beta g(u_h^{n,D}(x_{i-1/2}^{\beta,r},y_{j-1/2}))\\
=:&\frac{\theta}{4}H_1
\end{aligned}
$$

where the fourth equality is based on (26) and

$$
\begin{aligned}
H_1=&(1-\hat{\omega}_1)u_h^{n,D}(\xi_{i-1/2}^4,\eta_{j-1/2}^4)+\mu_1\sum_{\beta=1}^{3}\omega_\beta\hat{\omega}_1\left(u_h^{n,D}(x_{i-1/2},y_{j-1/2}^{\beta,r})+\frac{2\lambda_1}{\hat{\omega}_1\mu_1\theta}f(u_h^{n,D}(x_{i-1/2},y_{j-1/2}^{\beta,r}))\right)\\
&+\mu_2\sum_{\beta=1}^{3}\omega_\beta\hat{\omega}_1\left(u_h^{n,D}(x_{i-1/2}^{\beta,r},y_{j-1/2})+\frac{2\lambda_2}{\hat{\omega}_1\mu_2\theta}g(u_h^{n,D}(x_{i-1/2}^{\beta,r},y_{j-1/2}))\right).
\end{aligned}
$$

With the same approach, we can obtain the following relations

$$
\begin{aligned}
\theta U_2-\lambda_1F_2-\lambda_2G_2=:&\frac{\theta}{4}H_2,\\
\theta U_3-\lambda_1F_3-\lambda_2G_3=:&\frac{\theta}{4}H_3,\\
\theta U_4-\lambda_1F_4-\lambda_2G_4=:&\frac{\theta}{4}H_4,
\end{aligned}
$$

where H_2, H_3, H_4 can be obtained similarly as H_1.

Theorem 3.2. For the scheme (30), assume $\overline{u}_{ij}^{n,C}, \overline{u}_{i+1/2,j+1/2}^{n,D} \in [m,M]$, $\forall i,j$. If the values $u_h^{n,D}(x,y),(x,y) \in S_{i+1/2,j+1/2}$, $\forall i,j$, are in the range $[m,M]$, then $\overline{u}_{ij}^{n+1,C} \in [m,M]$, $\forall i,j$, under the CFL condition

$$
\lambda_1 a_1+\lambda_2 a_2 \leqslant \frac{\theta}{2}\hat{\omega}_1. \tag{31}
$$

Proof. The scheme (30) becomes

$$\overline{u}_{ij}^{n+1,C} = (1-\theta)\overline{u}_{ij}^{n,C} + \frac{\theta}{4}\left(H_1 + H_2 + H_3 + H_4\right) \tag{32}$$

Notice that $\overline{u}_{ij}^{n+1,C}$ is a convex combination of $\overline{u}_{ij}^{n,C}$ and H_k, $k = 1, \cdots, 4$. Therefore, to ensure $\overline{u}_{ij}^{n+1,C} \in [m, M]$, it suffices to enforce $H_k \in [m, M], k = 1, \cdots, 4$.

Each $H_k, k = 1, \cdots, 4$, is monotonically nondecreasing with respect to the corresponding point values $u_h^{n,D}(x, y), (x, y) \in S_{i+1/2,j+1/2}$, $\forall i, j$, and these values are in the range $[m, M]$. Based on the same procedure as in Theorem 3.1, one can verify that $H_k \in [m, M], k = 1, \cdots, 4$, if the CFL condition is satisfied.

□

Given $\overline{u}_{ij}^{n,C}, \overline{u}_{i+1/2,j+1/2}^{n,D} \in [m, M]$, the algorithm to update $\overline{u}_{ij}^{n+1,C}$ in the MPP central WENO scheme with Euler forward time discretization is:

1. Evaluate four quarter-cell averages

$$\frac{1}{\Delta x \Delta y}\int_{x_i}^{x_{i+1/2}}\int_{y_j}^{y_{j+1/2}} u_h^{n,D}(x,y)dxdy, \quad \frac{1}{\Delta x \Delta y}\int_{x_{i+1/2}}^{x_{i+1}}\int_{y_j}^{y_{j+1/2}} u_h^{n,D}(x,y)dxdy,$$
$$\frac{1}{\Delta x \Delta y}\int_{x_i}^{x_{i+1/2}}\int_{y_{j+1/2}}^{y_{j+1}} u_h^{n,D}(x,y)dxdy, \quad \frac{1}{\Delta x \Delta y}\int_{x_{i+1/2}}^{x_{i+1}}\int_{y_{j+1/2}}^{y_{j+1}} u_h^{n,D}(x,y)dxdy.$$

   and the point values

$$u_h^{n,D}(x,y),\ (x,y) \in \{(x_{i+1/2}, y) : y \in L^y\} \cup \{(x, y_{j+1/2}) : x \in L^x\},$$

   in each cell $I_{i+1/2,j+1/2}$ by the WENO reconstruction with a dimension-by-dimension procedure, where L^x and L^y are defined in (28).

2. Compute point values $u_h^{n,D}(x, y), (x, y) \in A$ by (23) - (26).

3. Modify the point values with the following MPP scaling limiter

$$\alpha = \min\left\{1, \left|\frac{M - \overline{u}_{i+1/2,j+1/2}^{n,D}}{M_{i+1/2,j+1/2} - \overline{u}_{i+1/2,j+1/2}^{n,D}}\right|, \left|\frac{m - \overline{u}_{i+1/2,j+1/2}^{n,D}}{m_{i+1/2,j+1/2} - \overline{u}_{i+1/2,j+1/2}^{n,D}}\right|\right\},$$

$$\widetilde{u}_h^{n,D}(x,y) = \alpha\left(u_h^{n,D}(x,y) - \overline{u}_{i+1/2,j+1/2}^{n,D}\right) + \overline{u}_{i+1/2,j+1/2}^{n,D}, \quad (x,y) \in S_{i+1/2,j+1/2},$$

with

$$M_{i+1/2,j+1/2} = \max_{(x,y)\in S_{i+1/2,j+1/2}} u_h^{n,D}(x,y), \quad m_{i+1/2,j+1/2} = \min_{(x,y)\in S_{i+1/2,j+1/2}} u_h^{n,D}(x,y).$$

4. Use $\widetilde{u}_h^{n,D}(x,y)$ instead of $u_h^{n,D}(x,y)$ in the central scheme (32) under the CFL condition (31).

4 Positivity-preserving central WENO schemes for compressible Euler equations

In this section, the positivity-preserving central WENO schemes for the compressible Euler equations are discussed. We only focus on the procedure to update $\overline{\mathbf{u}}_i^{n+1,C}$ and $\overline{\mathbf{u}}_{ij}^{n+1,C}$ in one- and two-dimensional case, and this similarly goes to $\overline{\mathbf{u}}_{i+1/2}^{n+1,D}$ and $\overline{\mathbf{u}}_{i+1/2,j+1/2}^{n+1,D}$.

4.1 One-dimensional case

Consider the one-dimensional compressible Euler equations

$$\mathbf{u}_t + \mathbf{f}(\mathbf{u})_x = 0, \tag{33}$$

with

$$\mathbf{u} = (\rho, m, E)^T, \ \mathbf{f}(\mathbf{u}) = (\rho u, \rho u^2 + p, (E+p)u)^T.$$

Here ρ is the density, u is the velocity, $m = \rho u$ is the momentum, p is the pressure, $E = \frac{1}{2}\rho u^2 + \frac{p}{\gamma - 1}$ is the total energy, and γ is the ratio of specific heat ($\gamma = 1.4$ for the air). The three eigenvalues of the Jacobian $\mathbf{f}'(\mathbf{u})$ are $u - c, u, u + c$ where $c = \sqrt{\frac{\gamma p}{\rho}}$ is the speed of sound.

In order to obtain the positivity-preserving scheme, one would like to define the set of admissible states by

$$G = \left\{\mathbf{u} = (\rho, m, E)^T : \rho > 0,\, p(\mathbf{u}) = (\gamma - 1)\left(E - \frac{m^2}{2\rho}\right) > 0\right\},$$

then G is a convex set [24].

Assume there is a vector of reconstructed polynomial $\mathbf{u}_h^{n,D}(x) = \left(\rho_h^{n,D}(x), m_h^{n,D}(x), E_h^{n,D}(x)\right)^T$ in the cell $I_{i+1/2}$ with the cell average

$$\frac{1}{\Delta x}\int_{x_i}^{x_{i+1}} \mathbf{u}_h^{n,D}(x)dx = \overline{\mathbf{u}}_{i+1/2}^{n,D} = \left(\overline{\rho}_{i+1/2}^{n,D}, \overline{m}_{i+1/2}^{n,D}, \overline{E}_{i+1/2}^{n,D}\right)^T.$$

The left and right half-cell averages of $\mathbf{u}_h^{n,D}(x)$ on cell $I_{i+1/2}$ are defined as follows,

$$\overline{\mathbf{u}}_{i+1/2}^{l} = \frac{1}{\Delta x}\int_{x_i}^{x_{i+1/2}} \mathbf{u}_h^{n,D}(x)dx, \quad \overline{\mathbf{u}}_{i+1/2}^{r} = \frac{1}{\Delta x}\int_{x_{i+1/2}}^{x_{i+1}} \mathbf{u}_h^{n,D}(x)dx = \overline{\mathbf{u}}_{i+1/2}^{n,D} - \overline{\mathbf{u}}_{i+1/2}^{l}.$$

Similarly as in (17)-(18), there exists $\xi_{i+1/2}^{l,1}, \xi_{i+1/2}^{l,2}, \xi_{i+1/2}^{l,3} \in [x_i, x_{i+1/2}]$ and $\xi_{i+1/2}^{r,1}, \xi_{i+1/2}^{r,2}, \xi_{i+1/2}^{r,3} \in [x_{i+1/2}, x_{i+1}]$, such that

$$\left(\rho_h^{n,D}(\xi_{i+1/2}^{l,1}), m_h^{n,D}(\xi_{i+1/2}^{l,2}), E_h^{n,D}(\xi_{i+1/2}^{l,3})\right)^T = \frac{1}{1-\hat{\omega}_4}\left(2\overline{\mathbf{u}}_{i+1/2}^{l} - \hat{\omega}_4 \mathbf{u}_h^{n,D}(x_{i+1/2})\right) \tag{34}$$

$$\left(\rho_h^{n,D}(\xi_{i+1/2}^{r,1}), m_h^{n,D}(\xi_{i+1/2}^{r,2}), E_h^{n,D}(\xi_{i+1/2}^{r,3})\right)^T = \frac{1}{1-\hat{\omega}_1}\left(2\overline{\mathbf{u}}_{i+1/2}^{r} - \hat{\omega}_1 \mathbf{u}_h^{n,D}(x_{i+1/2})\right) \tag{35}$$

where $\hat{\omega}_\alpha$ $(\alpha = 1, \cdots, 4)$ are the quadrature weights on the interval $[-\frac{1}{2}, \frac{1}{2}]$. Notice that $\xi_{i+1/2}^{l,1}$, $\xi_{i+1/2}^{l,2}$, $\xi_{i+1/2}^{l,3}$ and $\xi_{i+1/2}^{r,1}$, $\xi_{i+1/2}^{r,2}$, $\xi_{i+1/2}^{r,3}$ are three different points in $[x_i, x_{i+1/2}]$ and $[x_{i+1/2}, x_{i+1}]$, respectively. For convenience, we assume that $\mathbf{u}_h^{n,D}(x)$ is evaluated at one point and denote

$$\mathbf{u}_h^{n,D}(\xi_{i+1/2}^{l}) = \left(\rho_h^{n,D}(\xi_{i+1/2}^{l,1}), m_h^{n,D}(\xi_{i+1/2}^{l,2}), E_h^{n,D}(\xi_{i+1/2}^{l,3})\right)^T,$$
$$\mathbf{u}_h^{n,D}(\xi_{i+1/2}^{r}) = \left(\rho_h^{n,D}(\xi_{i+1/2}^{r,1}), m_h^{n,D}(\xi_{i+1/2}^{r,2}), E_h^{n,D}(\xi_{i+1/2}^{r,3})\right)^T.$$

Based on the procedure described in the equation (21), we shall now design the positivity-preserving central WENO scheme with the Euler forward in time. The scheme reads as

$$\begin{aligned}
\overline{\mathbf{u}}_i^{n+1,C} &= (1-\theta)\overline{\mathbf{u}}_i^{n,C} + \theta\frac{1}{\Delta x}\int_{I_i} \mathbf{u}_h^{n,D}(x)dx - \lambda\left[\mathbf{f}(\mathbf{u}_h^{n,D}(x_{i+1/2})) - \mathbf{f}(\mathbf{u}_h^{n,D}(x_{i-1/2}))\right] \\
&= (1-\theta)\overline{\mathbf{u}}_i^{n,C} + \frac{\theta}{2}\left((1-\hat{\omega}_1)\mathbf{u}_h^{n,D}(\xi_{i-1/2}^{r}) + (1-\hat{\omega}_4)\mathbf{u}_h^{n,D}(\xi_{i+1/2}^{l})\right) \\
&+ \frac{\theta\hat{\omega}_1}{2}\left(\mathbf{u}_h^{n,D}(x_{i-1/2}) + \frac{2\lambda}{\theta\hat{\omega}_1}\mathbf{f}(\mathbf{u}_h^{n,D}(x_{i-1/2}))\right) + \frac{\theta\hat{\omega}_4}{2}\left(\mathbf{u}_h^{n,D}(x_{i+1/2}) - \frac{2\lambda}{\theta\hat{\omega}_4}\mathbf{f}(\mathbf{u}_h^{n,D}(x_{i+1/2}))\right)
\end{aligned} \tag{36}$$

where $\lambda = \frac{\Delta t_n}{\Delta x}$. The sufficient condition for the scheme (36) to preserve the positivity can be summarized in the following theorem.

Theorem 4.1. For the scheme (36), assume $\overline{\mathbf{u}}_i^{n,C}, \overline{\mathbf{u}}_{i+1/2}^{n,D} \in G$, $\forall i$. If the values $\mathbf{u}_h^{n,D}(\xi_{i+1/2}^l)$, $\mathbf{u}_h^{n,D}(\xi_{i+1/2}^r), \mathbf{u}_h^{n,D}(x_{i+1/2}) \in G$, $\forall i$, then $\overline{\mathbf{u}}_i^{n+1,C} \in G$, $\forall i$, under the CFL condition

$$\lambda a \leqslant \frac{\theta}{2}\hat{\omega}_1. \tag{37}$$

where $a = \max\left(||(|u_h^{n,C}| + c^{n,C})||_\infty, ||(|u_h^{n,D}| + c^{n,D})||_\infty\right)$.

Proof. Notice that $\mathbf{u}_h^{n,D}(x_{i-1/2}), \mathbf{u}_h^{n,D}(x_{i+1/2})$ are in the set G. Under the CFL condition $\lambda a \leqslant \frac{\theta}{2}\hat{\omega}_1$, we can prove that $\mathbf{u}_h^{n,D}(x_{i-1/2}) + \frac{2\lambda}{\theta\hat{\omega}_1}\mathbf{f}(\mathbf{u}_h^{n,D}(x_{i-1/2}))$ and $\mathbf{u}_h^{n,D}(x_{i+1/2}) - \frac{2\lambda}{\theta\hat{\omega}_4}\mathbf{f}(\mathbf{u}_h^{n,D}(x_{i+1/2}))$ are also in the set G [24, 12]. Since $\overline{\mathbf{u}}_i^{n+1,C}$ is a convex combination of $\overline{\mathbf{u}}_i^{n,C}, \mathbf{u}_h^{n,D}(\xi_{i-1/2}^r)$, $\mathbf{u}_h^{n,D}(\xi_{i+1/2}^l)$, $\mathbf{u}_h^{n,D}(x_{i-1/2}) + \frac{2\lambda}{\theta\hat{\omega}_1}\mathbf{f}(\mathbf{u}_h^{n,D}(x_{i-1/2}))$ and $\mathbf{u}_h^{n,D}(x_{i+1/2}) - \frac{2\lambda}{\theta\hat{\omega}_4}\mathbf{f}(\mathbf{u}_h^{n,D}(x_{i+1/2}))$ which are all in the convex set G, therefore $\overline{\mathbf{u}}_i^{n+1,C} \in G$.

□

Given $\overline{\mathbf{u}}_i^{n,C}, \overline{\mathbf{u}}_{i+1/2}^{n,D} \in G$, the algorithm to update $\overline{\mathbf{u}}_i^{n+1,C}$ in the PP central WENO scheme with Euler forward time discretization is:

1. Evaluate the half-cell averages $\frac{1}{\Delta x}\int_{x_i}^{x_{i+1/2}} \mathbf{u}_h^{n,D}(x)dx$, $\frac{1}{\Delta x}\int_{x_{i+1/2}}^{x_{i+1}} \mathbf{u}_h^{n,D}(x)dx$, and the point value $\mathbf{u}_h^{n,D}(x_{i+1/2})$ based on the WENO reconstruction for each cell $I_{i+1/2}$.

2. Compute $\mathbf{u}_h^{n,D}(\xi_{i+1/2}^l)$ and $\mathbf{u}_h^{n,D}(\xi_{i+1/2}^r)$ by (34) - (35).

3. Set up a small number $\epsilon = \min_i\left\{10^{-13}, \overline{\rho}_{i+1/2}^{n,D}, p(\overline{\mathbf{u}}_{i+1/2}^{n,D})\right\}$.

4. Enforce the positivity of the density by the following PP limiter

$$\theta_1 = \min\left\{1, \left|\frac{\overline{\rho}_{i+1/2}^{n,D} - \epsilon}{\overline{\rho}_{i+1/2}^{n,D} - \rho_{\min}}\right|\right\}, \ \rho_{\min} = \min\left\{\rho_h^{n,D}(x_{i+1/2}), \rho_h^{n,D}(\xi_{i+1/2}^{l,1}), \rho_h^{n,D}(\xi_{i+1/2}^{r,1})\right\},$$

$$\widehat{\rho}_h^{n,D}(x) = \theta_1\left(\rho_h^{n,D}(x) - \overline{\rho}_{i+1/2}^{n,D}\right) + \overline{\rho}_{i+1/2}^{n,D}, \quad x \in \left\{x_{i+1/2}, \xi_{i+1/2}^{l,1}, \xi_{i+1/2}^{r,1}\right\}.$$

We define

$$\widehat{\mathbf{u}}_h^{n,D,1} = \widehat{\mathbf{u}}_h^{n,D}(x_{i+1/2}) = \left(\widehat{\rho}_h^{n,D}(x_{i+1/2}), m_h^{n,D}(x_{i+1/2}), E_h^{n,D}(x_{i+1/2})\right)^T,$$

$$\widehat{\mathbf{u}}_h^{n,D,2} = \widehat{\mathbf{u}}_h^{n,D}(\xi_{i+1/2}^l) = \left(\widehat{\rho}_h^{n,D}(\xi_{i+1/2}^{l,1}), m_h^{n,D}(\xi_{i+1/2}^{l,2}), E_h^{n,D}(\xi_{i+1/2}^{l,3})\right)^T,$$

$$\widehat{\mathbf{u}}_h^{n,D,3} = \widehat{\mathbf{u}}_h^{n,D}(\xi_{i+1/2}^r) = \left(\widehat{\rho}_h^{n,D}(\xi_{i+1/2}^{r,1}), m_h^{n,D}(\xi_{i+1/2}^{r,2}), E_h^{n,D}(\xi_{i+1/2}^{r,3})\right)^T.$$

5. Enforce the positivity of the pressure of $\widehat{\mathbf{u}}_h^{n,D,l}, l = 1, 2, 3$ with the following PP limiter

$$\theta_2 = \min_{l=1,2,3}\{t^l\}, \quad t^l = \begin{cases} 1, & p(\widehat{\mathbf{u}}_h^{n,D,l}) \geq \epsilon, \\ \frac{p(\overline{\mathbf{u}}_{i+1/2}^{n,D})-\epsilon}{p(\overline{\mathbf{u}}_{i+1/2}^{n,D})-p(\widehat{\mathbf{u}}_h^{n,D,l})}, & \text{otherwise}, \end{cases} \quad l = 1, 2, 3,$$

$$\widetilde{\mathbf{u}}_h^{n,D}(x) = \theta_2 \left(\widehat{\mathbf{u}}_h^{n,D}(x) - \overline{\mathbf{u}}_{i+1/2}^{n,D}\right) + \overline{\mathbf{u}}_{i+1/2}^{n,D}, \quad x \in \left\{x_{i+1/2},\, \xi_{i+1/2}^l,\, \xi_{i+1/2}^r\right\}.$$

6. Use $\widetilde{\mathbf{u}}_h^{n,D}(x)$ instead of $\mathbf{u}_h^{n,D}(x)$ in the central scheme (36) under the CFL condition (37).

Remark 1. For the system case, the local characteristic decomposition is applied in the half-cell average reconstructions to enhance non-oscillatory property of the scheme. The remaining reconstructions for the point values are implemented in a componentwise manner.

4.2 Two-dimensional case

Consider the two-dimensional compressible Euler equations

$$\mathbf{u}_t + \mathbf{f}(\mathbf{u})_x + \mathbf{g}(\mathbf{u})_y = 0, \tag{38}$$

with

$$\mathbf{u} = (\rho, m, n, E)^T,\ \mathbf{f}(\mathbf{u}) = (\rho u, \rho u^2 + p, \rho uv, (E+p)u)^T,\ \mathbf{g}(\mathbf{u}) = (\rho v, \rho uv, \rho v^2 + p, (E+p)v)^T.$$

Here ρ is the density, u is the velocity in x direction and v is the velocity in y direction, $m = \rho u$ and $n = \rho v$ are the momentums, p is the pressure, $E = \frac{1}{2}\rho u^2 + \frac{1}{2}\rho v^2 + \frac{p}{\gamma-1}$ is the total energy. The speed of sound is still defined as $c = \sqrt{\frac{\gamma p}{\rho}}$. The four eigenvalues of the Jacobian $\mathbf{f}'(\mathbf{u})$ and $\mathbf{g}'(\mathbf{u})$ are $u - c, u, u, u + c$ and $v - c, v, v, v + c$, respectively. We would like to define the set of admissible states for the two-dimensional Euler equations as

$$G = \left\{\mathbf{u} = (\rho, m, n, E)^T : \rho > 0,\, p(\mathbf{u}) = (\gamma - 1)\left(E - \frac{m^2 + n^2}{2\rho}\right) > 0\right\},$$

then G is still convex.

Let's consider the central WENO scheme with the Euler forward in time

$$\begin{aligned}\overline{\mathbf{u}}_{ij}^{n+1,C} =&(1-\theta)\overline{\mathbf{u}}_{ij}^{n,C} + \frac{\theta}{\Delta x\Delta y}\int_{I_{ij}} \mathbf{u}_h^{n,D}(x,y)dxdy \\ &- \frac{\lambda_1}{\Delta y}\int_{y_{j-1/2}}^{y_{j+1/2}} \left[\mathbf{f}(\mathbf{u}_h^{n,D}(x_{i+1/2},y)) - \mathbf{f}(\mathbf{u}_h^{n,D}(x_{i-1/2},y))\right] dy \\ &- \frac{\lambda_2}{\Delta x}\int_{x_{i-1/2}}^{x_{i+1/2}} \left[\mathbf{g}(\mathbf{u}_h^{n,D}(x,y_{j+1/2})) - \mathbf{g}(\mathbf{u}_h^{n,D}(x,y_{j-1/2}))\right] dx \end{aligned} \tag{39}$$

where $\lambda_1 = \frac{\Delta t_n}{\Delta x}, \lambda_2 = \frac{\Delta t_n}{\Delta y}$ and the integrals in (39) are approximated by the same Gauss-Lobatto or Gauss quadrature in Section 3.2. Following the similar procedure as in Section 3.2, one can obtain the system-version of the central WENO scheme (32) which is still referred to as (39), and the following result holds.

Theorem 4.2. For the scheme (39), assume $\overline{\mathbf{u}}_{ij}^{n,C}, \overline{\mathbf{u}}_{i+1/2,j+1/2}^{n,D} \in G$, $\forall i,j$. If the values $\mathbf{u}_h^{n,D}(x,y) \in G, (x,y) \in S_{i+1/2,j+1/2}$, $\forall i,j$, then $\overline{\mathbf{u}}_{ij}^{n+1,C} \in G$, $\forall i,j$, under the CFL condition

$$\lambda_1 a_1 + \lambda_2 a_2 \leqslant \frac{\theta}{2}\hat{\omega}_1. \tag{40}$$

where

$$a_1 = \max\left(||(|u_h^{n,C}| + c^{n,C})||_\infty, ||(|u_h^{n,D}| + c^{n,D})||_\infty\right), \tag{41}$$

$$a_2 = \max\left(||(|v_h^{n,C}| + c^{n,C})||_\infty, ||(|v_h^{n,D}| + c^{n,D})||_\infty\right), \tag{42}$$

and $S_{i+1/2,j+1/2}$ is defined in (29).

Given $\overline{\mathbf{u}}_{ij}^{n,C}, \overline{\mathbf{u}}_{i+1/2,j+1/2}^{n,D} \in G$, the algorithm to update $\overline{\mathbf{u}}_{ij}^{n+1,C}$ in the PP central WENO scheme with Euler forward time discretization is:

1. Evaluate the four quarter-cell averages

$$\frac{1}{\Delta x\Delta y}\int_{x_i}^{x_{i+1/2}}\int_{y_j}^{y_{j+1/2}} \mathbf{u}_h^{n,D}(x,y)dxdy, \quad \frac{1}{\Delta x\Delta y}\int_{x_{i+1/2}}^{x_{i+1}}\int_{y_j}^{y_{j+1/2}} \mathbf{u}_h^{n,D}(x,y)dxdy,$$
$$\frac{1}{\Delta x\Delta y}\int_{x_i}^{x_{i+1/2}}\int_{y_{j+1/2}}^{y_{j+1}} \mathbf{u}_h^{n,D}(x,y)dxdy, \quad \frac{1}{\Delta x\Delta y}\int_{x_{i+1/2}}^{x_{i+1}}\int_{y_{j+1/2}}^{y_{j+1}} \mathbf{u}_h^{n,D}(x,y)dxdy.$$

and the point values

$$\mathbf{u}_h^{n,D}(x,y),\ (x,y) \in \{(x_{i+1/2},y) : y \in L^y\} \cup \{(x,y_{j+1/2}) : x \in L^x\},$$

in each cell $I_{i+1/2,j+1/2}$ by the WENO reconstruction with a dimension-by-dimension approach, where L^x and L^y are defined in (28).

2. Compute point values $\mathbf{u}_h^{n,D}(x,y), (x,y) \in A$, where A is defined in (27).

3. Set up a small number $\epsilon = \min_i \left\{ 10^{-13}, \overline{\rho}_{i+1/2,j+1/2}^{n,D}, p(\overline{\mathbf{u}}_{i+1/2,j+1/2}^{n,D}) \right\}$.

4. Enforce the positivity of the density by the following PP limiter

$$\theta_1 = \min\left\{1, \left|\frac{\overline{\rho}_{i+1/2,j+1/2}^{n,D} - \epsilon}{\overline{\rho}_{i+1/2,j+1/2}^{n,D} - \rho_{\min}}\right|\right\}, \ \rho_{\min} = \min_{(x,y)\in S_{i+1/2,j+1/2}} \left\{\rho_h^{n,D}(x,y)\right\},$$

$$\widehat{\rho}_h^{n,D}(x,y) = \theta_1\left(\rho_h^{n,D}(x,y) - \overline{\rho}_{i+1/2,j+1/2}^{n,D}\right) + \overline{\rho}_{i+1/2,j+1/2}^{n,D}, \quad (x,y) \in S_{i+1/2,j+1/2}.$$

We set

$$\widehat{\mathbf{u}}_h^{n,D}(x,y) = \left(\widehat{\rho}_h^{n,D}(x,y), m_h^{n,D}(x,y), n_h^{n,D}(x,y), E_h^{n,D}(x,y)\right)^T, \quad (x,y) \in S_{i+1/2,j+1/2}.$$

For convenience, we still assume that $\widehat{\mathbf{u}}_h^{n,D}(x,y)$ is evaluated at one point when

$$(x,y) \in \left\{(\xi_{i+1/2}^1, \eta_{j+1/2}^1), (\xi_{i+1/2}^2, \eta_{j+1/2}^2), (\xi_{i+1/2}^3, \eta_{j+1/2}^3), (\xi_{i+1/2}^4, \eta_{j+1/2}^4)\right\}.$$

5. Enforce the positivity of the pressure with the following PP limiter

$$\theta_2 = \min_{(x,y)\in S_{i+1/2,j+1/2}} \{t(x,y)\},$$

$$t(x,y) = \begin{cases} 1, & p\left(\widehat{\mathbf{u}}_h^{n,D}(x,y)\right) \geq \epsilon, \\ \frac{p\left(\overline{\mathbf{u}}_{i+1/2,j+1/2}^{n,D}\right) - \epsilon}{p\left(\overline{\mathbf{u}}_{i+1/2,j+1/2}^{n,D}\right) - p\left(\widehat{\mathbf{u}}_h^{n,D}(x,y)\right)}, & \text{otherwise}, \end{cases} \quad (x,y) \in S_{i+1/2,j+1/2},$$

$$\widetilde{\mathbf{u}}_h^{n,D}(x,y) = \theta_2\left(\widehat{\mathbf{u}}_h^{n,D}(x,y) - \overline{\mathbf{u}}_{i+1/2,j+1/2}^{n,D}\right) + \overline{\mathbf{u}}_{i+1/2,j+1/2}^{n,D}, \quad (x,y) \in S_{i+1/2,j+1/2}.$$

6. Use $\widetilde{\mathbf{u}}_h^{n,D}(x,y)$ instead of $\mathbf{u}_h^{n,D}(x,y)$ in the central scheme (39) under the CFL condition (40).

4.3 The implementation of SSP Runge-Kutta time discretization

For the time discretization, the third-order SSP Runge-Kutta method (16) is applied in our computation. Such method is a convex combination of Euler forward method, and therefore the maximum principle or positivity properties are still preserved with the high-order time discretization.

We take the PP central WENO scheme in Section 4.2 as an example to discuss the implementation of the third-order SSP Runge-Kutta method. In fact, the CFL condition (40) is sufficient rather than necessary for $\overline{\mathbf{u}}_{ij}^{n+1,C}, \overline{\mathbf{u}}_{i+1/2,j+1/2}^{n+1,D} \in G$. Therefore, one can start the computation with a larger CFL number. If the negative density or pressure occurs, we could return to the first stage of the Runge-Kutta method and restart the computation with a half time step. The algorithm to update $\overline{\mathbf{u}}_{ij}^{n+1,C}$ and $\overline{\mathbf{u}}_{i+1/2,j+1/2}^{n+1,D}$ in the Section 4.2 with the third-order SSP Runge-Kutta method can be implemented as follows:

1. Given $\overline{\mathbf{u}}_{ij}^{n,C}, \overline{\mathbf{u}}_{i+1/2,j+1/2}^{n,D} \in G$, compute a_1 and a_2 in (41)-(42) by taking the maximum over $\overline{\mathbf{u}}_{ij}^{n,C}$ and $\overline{\mathbf{u}}_{i+1/2,j+1/2}^{n,D}$ for all i, j.

2. Compute the time step $\Delta t_n = \frac{C_{cfl}}{\frac{a_1}{\Delta x}+\frac{a_2}{\Delta y}}$ with a larger CFL number C_{cfl} than the CFL condition (40) and C_{cfl} will be specified in Section 5.

3. Compute the first stage of the Runge-Kutta method, denoted as $\overline{\mathbf{u}}_{ij}^{(1),C}$ and $\overline{\mathbf{u}}_{i+1/2,j+1/2}^{(1),D}$.

   - If the cell averages $\overline{\mathbf{u}}_{ij}^{(1),C}, \overline{\mathbf{u}}_{i+1/2,j+1/2}^{(1),D} \in G$, then go to step 4.
   - If the cell averages $\overline{\mathbf{u}}_{ij}^{(1),C}$ or $\overline{\mathbf{u}}_{i+1/2,j+1/2}^{(1),D}$ contain negative density or pressure, then set $\Delta t_n = \frac{\Delta t_n}{2}$ and recompute the first stage.

4. Given $\overline{\mathbf{u}}_{ij}^{(1),C}, \overline{\mathbf{u}}_{i+1/2,j+1/2}^{(1),D} \in G$, compute the second stage of the Runge-Kutta method, denoted as $\overline{\mathbf{u}}_{ij}^{(2),C}$ and $\overline{\mathbf{u}}_{i+1/2,j+1/2}^{(2),D}$.

   - If the cell averages $\overline{\mathbf{u}}_{ij}^{(2),C}, \overline{\mathbf{u}}_{i+1/2,j+1/2}^{(2),D} \in G$, then go to step 5.
   - If the cell averages $\overline{\mathbf{u}}_{ij}^{(2),C}$ or $\overline{\mathbf{u}}_{i+1/2,j+1/2}^{(2),D}$ contain negative density or pressure, then go to step 3 and restart the computation with $\Delta t_n = \frac{\Delta t_n}{2}$.

5. Given $\overline{\mathbf{u}}_{ij}^{(2),C}, \overline{\mathbf{u}}_{i+1/2,j+1/2}^{(2),D} \in G$, compute the solution at time level t^{n+1}, denoted as $\overline{\mathbf{u}}_{ij}^{n+1,C}$ and $\overline{\mathbf{u}}_{i+1/2,j+1/2}^{n+1,D}$.

   - If the cell averages $\overline{\mathbf{u}}_{ij}^{n+1,C}, \overline{\mathbf{u}}_{i+1/2,j+1/2}^{n+1,D} \in G$, this completes the loop from t^n to t^{n+1}.
   - If the cell averages $\overline{\mathbf{u}}_{ij}^{n+1,C}$ or $\overline{\mathbf{u}}_{i+1/2,j+1/2}^{n+1,D}$ contain negative density or pressure, then go to step 3 and restart the computation with $\Delta t_n = \frac{\Delta t_n}{2}$.

Remark 2. Based on the Theorem 4.2, the above algorithm will stop once the time step is sufficient small.

5 Numerical experiments

In this section, the high-order accuracy and performance of the proposed methods are illustrated by numerical tests. The numerical results on primal mesh are reported and the solutions can be either smooth or non-smooth. Although the parameter θ in the schemes (3)-(4) and (11)-(12) can be chosen from $[0, 1]$, we take $\theta = 1$ in our computation for the efficiency.

The time step Δt_n is set as

$$\Delta t_n = C_{cfl}\frac{\Delta x}{a},$$

in one-dimensional case, and we take

$$\Delta t_n = \frac{C_{cfl}}{\frac{a_1}{\Delta x} + \frac{a_2}{\Delta y}},$$

in two-dimensional case. For the non-smooth problems, the CFL number C_{cfl} is taken as 0.45 for one-dimensional tests, and 0.2 for two-dimensional ones. For the accuracy test of smooth problems, C_{cfl} is set to be $\frac{1}{24}$ to ensure the spatial errors dominate.

5.1 Scalar conservation laws

The numerical results by the MPP central WENO schemes are shown to simulate the scalar conservation laws. Without the MPP limiter, the schemes might violate the MPP property.

Example 5.1 (1D linear equation). Consider the one-dimensional linear equation

$$u_t + u_x = 0$$

with the initial condition $u(x,0) = sin^4(x)$ on $[0, 2\pi]$ and a periodic boundary condition. The solution is computed up to $T = 0.5$. We present the L^1 and L^∞ errors and orders of accuracy in Tables 1 - 2. Both schemes achieve their designed fifth-order accuracy. The minimum and maximum values of numerical solutions are also listed in the tables. We observe that the minimum values are strictly non-negative by the scheme with limiter, while the minimum values without limiter are negative.

Then, the initial condition is taken as

$$u_0(x) = \begin{cases} 1, & 0.25 \le x \le 0.75, \\ 0, & \text{otherwise}, \end{cases} \tag{43}$$

on $[0, 1]$ with a periodic boundary condition. We compute the solution up to $T = 1.0$ without and with limiter. The minimum and maximum values of numerical solutions are shown in Table 3. One can find that the solution without limiter will be beyond the range $[0, 1]$, while the solution with limiter are bounded in $[0, 1]$.

Table 1: 1D linear equation with initial condition $u(x,0) = sin^4(x)$, without limiter. $T = 0.5$.

N	L^1 error	order	L^∞ error	order	$(u_h)_{min}$	$(u_h)_{max}$
20	5.11e-02		1.07e-01		-3.90e-02	0.87504
40	3.27e-03	3.96	7.12e-03	3.91	-3.93e-03	0.98388
80	2.29e-04	3.84	5.89e-04	3.59	-4.95e-04	0.99856
160	8.10e-06	4.82	3.17e-05	4.22	-1.41e-05	0.99957
320	2.31e-07	5.13	9.43e-07	5.07	-8.16e-08	0.99993
640	5.61e-09	5.36	1.54e-08	5.93	-1.31e-09	0.99995

Table 2: 1D linear equation with initial condition $u_0(x) = sin^4(x)$, with limiter. $T = 0.5$.

N	L^1 error	order	L^∞ error	order	$(u_h)_{min}$	$(u_h)_{max}$
20	4.40e-02		1.06e-01		4.04e-04	0.87654
40	2.76e-03	4.00	7.17e-03	3.88	1.07e-04	0.98384
80	1.72e-04	4.01	3.53e-04	4.34	1.65e-07	0.99856
160	7.40e-06	4.54	2.81e-05	3.65	4.85e-08	0.99957
320	2.31e-07	5.00	9.40e-07	4.90	7.76e-09	0.99993
640	5.70e-09	5.34	1.80e-08	5.71	5.52e-10	0.99995

Table 3: Minimum and maximum values for the 1D linear equation with discontinuous initial condition (43). $T = 1.0$.

N	without limiter		with limiter	
	$(u_h)_{min}$	$(u_h)_{max}$	$(u_h)_{min}$	$(u_h)_{max}$
80	-3.89e-03	1.00393	5.18e-10	1.00000
160	-3.47e-03	1.00346	1.38e-15	1.00000
320	-4.22e-03	1.00420	1.27e-25	1.00000
640	-7.29e-03	1.00731	3.72e-46	1.00000

Example 5.2 (1D Burgers' equation). Consider the one-dimensional nonlinear Burgers' equation

$$u_t + \left(\frac{u^2}{2}\right)_x = 0$$

with the initial value $u_0(x) = sin^4(x)$ on $[0, 2\pi]$ and a periodic boundary condition. The final time is $T = 0.5$ and the exact solution is smooth up to $t = \frac{4\sqrt{3}}{9} \approx 0.7698$. The L^1 and L^∞ errors and orders of accuracy without and with limiter are shown in Tables 4-5. Both schemes achieve their designed fifth-order accuracy. Note that the solutions by the scheme with limiter are bounded in $[0, 1]$, but the scheme without limiter will generate negative solutions.

The solution develops shocks after $t = \frac{4\sqrt{3}}{9}$ and is computed up to $T = 1.2$. We remove about 7.5% of the total mesh elements at each shock and show the L^1 and L^∞ errors with orders of accuracy in Table 6. The fifth-order accuracy is obtained for the smooth region of the discontinuous solution. In Table 7, we present the minimum and maximum values of the numerical solutions for the schemes without and with limiter. Again, the solutions without limiter violate the MPP property, and the solutions with limiter are satisfactory.

Table 4: 1D Burgers' equation with initial condition $u_0(x) = sin^4(x)$, without limiter. $T = 0.5$.

N	L^1 error	order	L^∞ error	order	$(u_h)_{min}$	$(u_h)_{max}$
20	4.53e-02		1.43e-01		-2.55e-02	0.84594
40	1.13e-02	2.01	6.75e-02	1.09	-4.27e-03	0.97376
80	1.85e-03	2.61	2.07e-02	1.71	-4.48e-04	0.99956
160	2.38e-04	2.96	4.35e-03	2.25	-1.31e-05	0.99945
320	1.48e-05	4.01	4.07e-04	3.42	-6.36e-08	0.99992
640	5.56e-07	4.73	1.91e-05	4.42	-8.39e-10	0.99995
1280	1.79e-08	4.96	6.53e-07	4.87	3.39e-11	0.99999

Table 5: 1D Burgers' equation with initial condition $u_0(x) = sin^4(x)$, with limiter. $T = 0.5$.

N	L^1 error	order	L^∞ error	order	$(u_h)_{min}$	$(u_h)_{max}$
20	4.34e-02		1.44e-01		8.50e-04	0.83972
40	1.05e-02	2.05	6.76e-02	1.09	3.20e-04	0.97381
80	1.78e-03	2.56	2.07e-02	1.71	2.70e-06	0.99931
160	2.37e-04	2.91	4.35e-03	2.25	2.83e-07	0.99945
320	1.48e-05	4.00	4.07e-04	3.42	3.05e-09	0.99992
640	5.56e-07	4.73	1.91e-05	4.42	1.05e-09	0.99995
1280	1.79e-08	4.96	6.53e-07	4.87	8.35e-11	0.99999

Table 6: 1D Burgers' equation with initial condition $u_0(x) = sin^4(x)$. $T = 1.2$.

N	without limiter				with limiter			
	L^1 error	order	L^∞ error	order	L^1 error	order	L^∞ error	order
80	2.69e-03		6.25e-02		2.63e-03		6.28e-02	
160	1.05e-04	4.68	3.07e-03	4.35	1.03e-04	4.67	3.08e-03	4.35
320	9.49e-06	3.46	6.98e-04	2.14	9.52e-06	3.44	7.03e-04	2.13
640	9.83e-08	6.59	1.02e-05	6.09	9.71e-08	6.62	1.04e-05	6.08

Table 7: Minimum and maximum values for the 1D Burgers' equation with initial condition $u_0(x) = sin^4(x)$. $T = 1.2$.

N	without limiter		with limiter	
	$(u_h)_{min}$	$(u_h)_{max}$	$(u_h)_{min}$	$(u_h)_{max}$
80	-1.11e-03	0.94299	5.92e-06	0.94288
160	-4.45e-05	0.97134	2.13e-06	0.97134
320	-7.49e-07	0.98772	5.51e-08	0.98772
640	-5.04e-09	0.99468	3.11e-10	0.99469

Example 5.3 (2D Burgers' equation). Consider the nonlinear Burgers' equation in two dimensions

$$u_t + \left(\frac{u^2}{2}\right)_x + \left(\frac{u^2}{2}\right)_y = 0$$

with the initial value $u_0(x, y) = sin^4(x + y)$ on $[0, 2\pi] \times [0, 2\pi]$ and periodic boundary conditions. We compute the solution up to $T = 0.2$. The L^1 and L^∞ errors and orders of accuracy without and with limiter are reported in Tables 8-9. The results are similar to the one-dimensional case.

In Table 10, we present the minimum and maximum values of the discontinuous solutions at $T = 0.8$ for the schemes without and with limiter. We can observe that the minimum values of the solutions without limiter are negative, whereas the solutions with limiter are maximum-principle-preserving.

Table 8: 2D Burgers' equation with initial condition $u_0(x, y) = sin^4(x + y)$, without limiter. $T = 0.2$.

$N_x \times N_y$	L^1 error	order	L^∞ error	order	$(u_h)_{min}$	$(u_h)_{max}$
20 × 20	6.12e-02		1.34e-01		-3.47e-02	0.83357
40 × 40	1.02e-02	2.58	4.88e-02	1.45	-6.24e-03	0.97385
80 × 80	1.36e-03	2.92	1.07e-02	2.19	-6.05e-04	0.99835
160 × 160	1.12e-04	3.60	1.37e-03	2.96	-2.14e-05	0.99926
320 × 320	4.88e-06	4.52	8.30e-05	4.05	-1.29e-07	0.99976
640 × 640	1.61e-07	4.92	2.93e-06	4.82	-3.48e-09	0.99995

Table 9: 2D Burgers' equation with initial condition $u_0(x, y) = sin^4(x + y)$, with limiter. $T = 0.2$.

$N_x \times N_y$	L^1 error	order	L^∞ error	order	$(u_h)_{min}$	$(u_h)_{max}$
20 × 20	5.63e-02		1.33e-01		3.85e-03	0.82988
40 × 40	8.99e-03	2.65	4.87e-02	1.45	3.73e-05	0.97389
80 × 80	1.29e-03	2.80	1.07e-02	2.19	2.23e-06	0.99817
160 × 160	1.10e-04	3.55	1.37e-03	2.96	2.12e-07	0.99926
320 × 320	4.89e-06	4.50	8.30e-05	4.05	1.90e-08	0.99976
640 × 640	1.62e-07	4.91	2.93e-06	4.82	1.78e-10	0.99995

Table 10: Minimum and maximum values for the 2D Burgers' equation with initial condition $u_0(x,y) = sin^4(x+y)$. $T = 0.8$.

$N_x \times N_y$	without limiter		with limiter	
	$(u_h)_{min}$	$(u_h)_{max}$	$(u_h)_{min}$	$(u_h)_{max}$
80 × 80	4.28e-04	0.89199	5.80e-04	0.89198
160 × 160	-1.91e-04	0.92283	5.68e-06	0.92282
320 × 320	-1.14e-04	0.93794	5.34e-07	0.93794
640 × 640	-1.38e-08	0.94728	5.15e-09	0.94728

5.2 Compressible Euler equations

The numerical results by the PP central WENO schemes are provided to simulate the compressible Euler equations. Without the PP limiter, the scheme might blow up for some examples.

Example 5.4 (**Accuracy test).** Consider the vortex evolution problem of the two-dimensional Euler equations (38). The mean flow is $\rho = u = v = p = 1$. Add to the mean flow an isentropic vortex perturbation centered at (x_0, y_0) in (u, v) and $T = \frac{p}{\rho}$, no perturbation in $S = \frac{p}{\rho^\gamma}$,

$$(\delta u, \delta v) = \frac{\epsilon}{2\pi} e^{0.5(1-r^2)}(-\bar{y}, \bar{x}), \quad \delta T = -\frac{(\gamma-1)\epsilon^2}{8\gamma\pi^2} e^{(1-r^2)}, \quad \delta S = 0,$$

where $(\bar{x}, \bar{y}) = (x - x_0, y - y_0), r^2 = \bar{x}^2 + \bar{y}^2$.

The computational domain is $[-5, 15] \times [-5, 15]$ and $(x_0, y_0) = (5, 5)$. The periodic boundary condition is applied in each direction. The exact solution is the passive convection of the vortex with the mean velocity. We set $\gamma = 1.4$ and the vortex strength $\epsilon = 10.0828$ such that the lowest density and pressure of the exact solution are 7.8×10^{-15} and 1.7×10^{-20}, respectively. The L^1 and L^∞ errors and orders of accuracy as well as the minimum values of density and pressure at $T = 0.05$ are reported in Table 11. Our scheme achieves the designed fifth-order accuracy without any negative density or pressure. For each time step, the percentage of the cells where PP limiter was activated is reported in Table 11 as well.

Next, we consider three one-dimensional low density and low pressure problems of (33) for ideal gas.

Table 11: The vortex evolution problem of two-dimensional Euler equations with PP limiter. $T = 0.05$.

$N_x \times N_y$	L^1 error	order	L^∞ error	order	ρ_{min}	p_{min}	limited (%)
100 × 100	1.07e-04		1.01e-02		5.01e-03	3.33e-04	≤ 0.077
200 × 200	2.25e-05	2.26	4.70e-03	1.11	3.79e-04	5.16e-07	≤ 0.032
400 × 400	1.39e-06	4.01	7.08e-04	2.73	8.00e-05	2.83e-07	≤ 0.023
800 × 800	3.18e-08	5.46	1.59e-05	5.48	1.75e-06	1.96e-07	≤ 0.001
1600 × 1600	4.60e-10	6.11	1.98e-07	6.32	1.01e-07	3.31e-09	≤ 0.001

Example 5.5 (**1D double rarefaction problem).** Consider the one-dimensional double rarefaction problem of (33). The initial condition for this Riemann problem is

$$(\rho, u, p, \gamma) = \begin{cases} (7, -1, 0.2, 1.4), & x \in [-1, 0), \\ (7, 1, 0.2, 1.4), & x \in [0, 1]. \end{cases}$$

The outflow boundary condition is applied to both ends. We compute up to $T = 0.6$ and the percentage of the cells where PP limiter was activated is less than 0.003%. The numerical solutions are shown in Figure 1 with $N = 400$ mesh elements, together with the exact solutions. We can see that the low density and pressure are captured very well with positivity.

Example 5.6 (**1D Sedov problem).** Consider the one-dimensional Sedov blast wave of (33). For the initial condition, the density is 1, velocity is 0, total energy is 10^{-12} everywhere except that the energy in the center cell is the constant $\frac{3{,}200{,}000}{\Delta x}$ (emulating a δ-function at the center). The computational domain is $[-2, 2]$ with an outflow boundary condition and $\gamma = 1.4$. ε in the nonlinear weights of WENO reconstruction is chosen to be 10^{-20} for this extreme problem. We compute the solution up to $T = 0.001$ and the percentage of the cells where PP limiter was activated is less than 0.003%. The numerical solutions are shown in Figure 2 with $N = 400$ mesh elements, together with the exact solutions. We can observe that our results match well with the exact solutions.

Example 5.7 (**1D Leblanc problem).** Consider the one-dimensional Leblanc problem of (33). The initial condition for this Riemann problem is

$$(\rho, u, p, \gamma) = \begin{cases} (2, 0, 10^9, 1.4), & x \in [-10, 0), \\ (0.001, 0, 1, 1.4), & x \in [0, 10]. \end{cases}$$

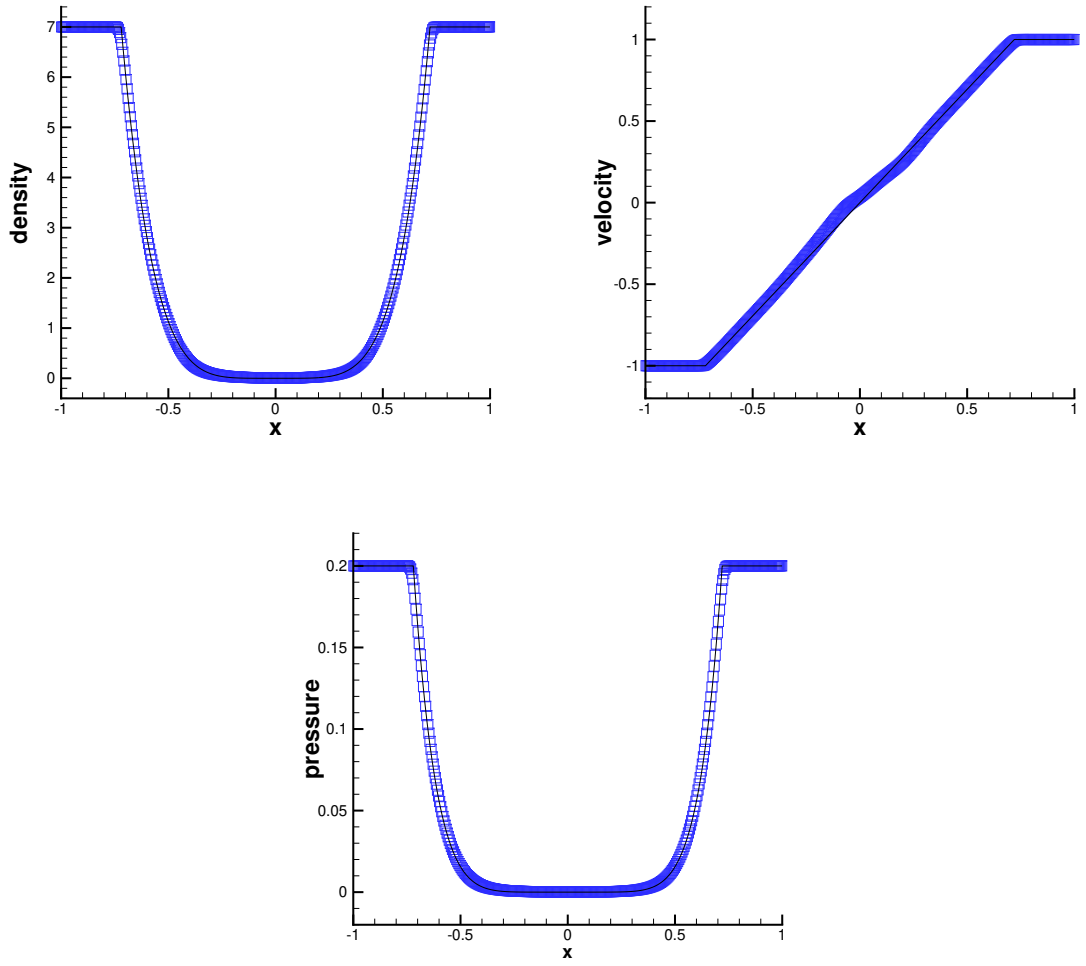

Figure 1: One-dimensional double rarefaction problem. $T = 0.6$ and $N = 400$. Solid line: exact solutions; square: numerical solutions.

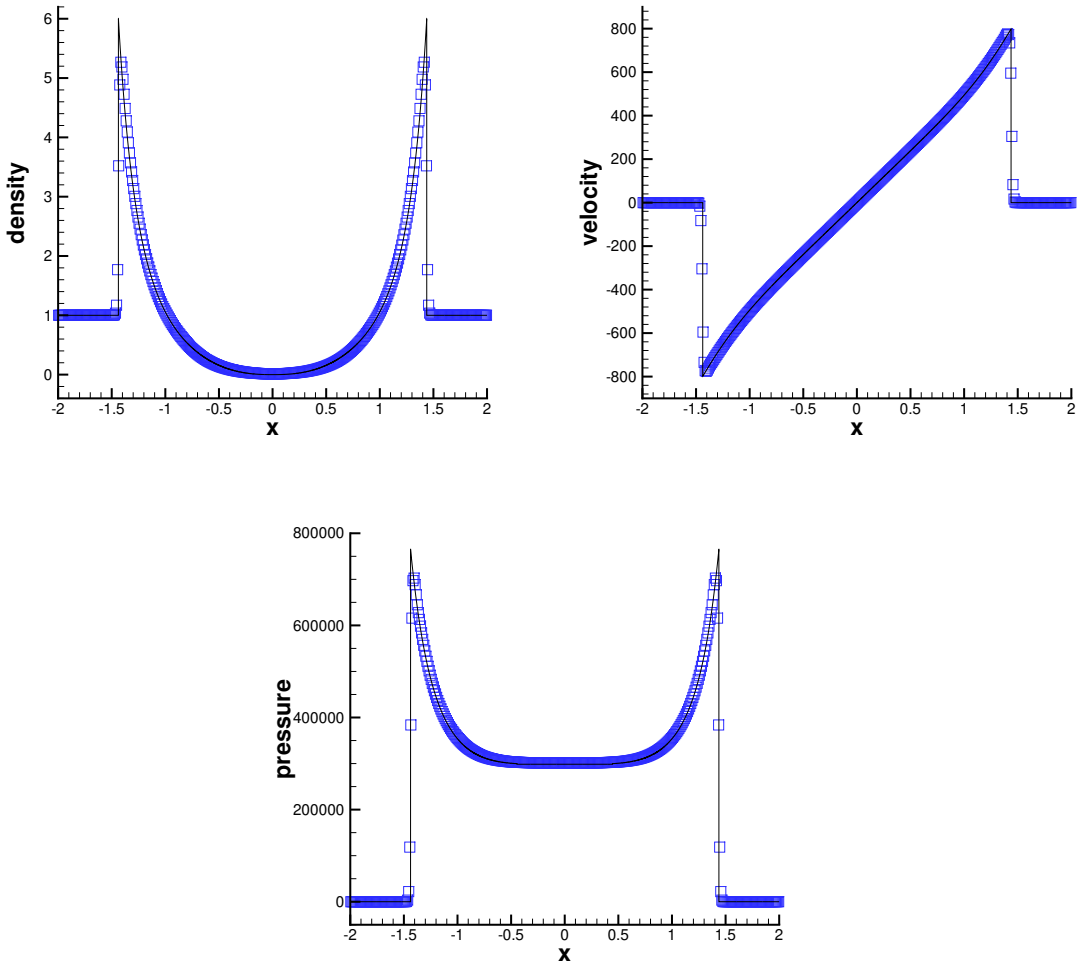

Figure 2: One-dimensional Sedov problem. $T = 0.001$ and $N = 400$. Solid line: exact solutions; square: numerical solutions.

The inflow/outflow boundary conditions are applied to left/right ends. We compute the solution up to $T = 0.0001$. The numerical solutions are plotted in Figure 3 with $N = 800$ mesh elements, together with the exact solutions. Notice that the discontinuity in the pressure are very large, and the shock is captured well by our method.

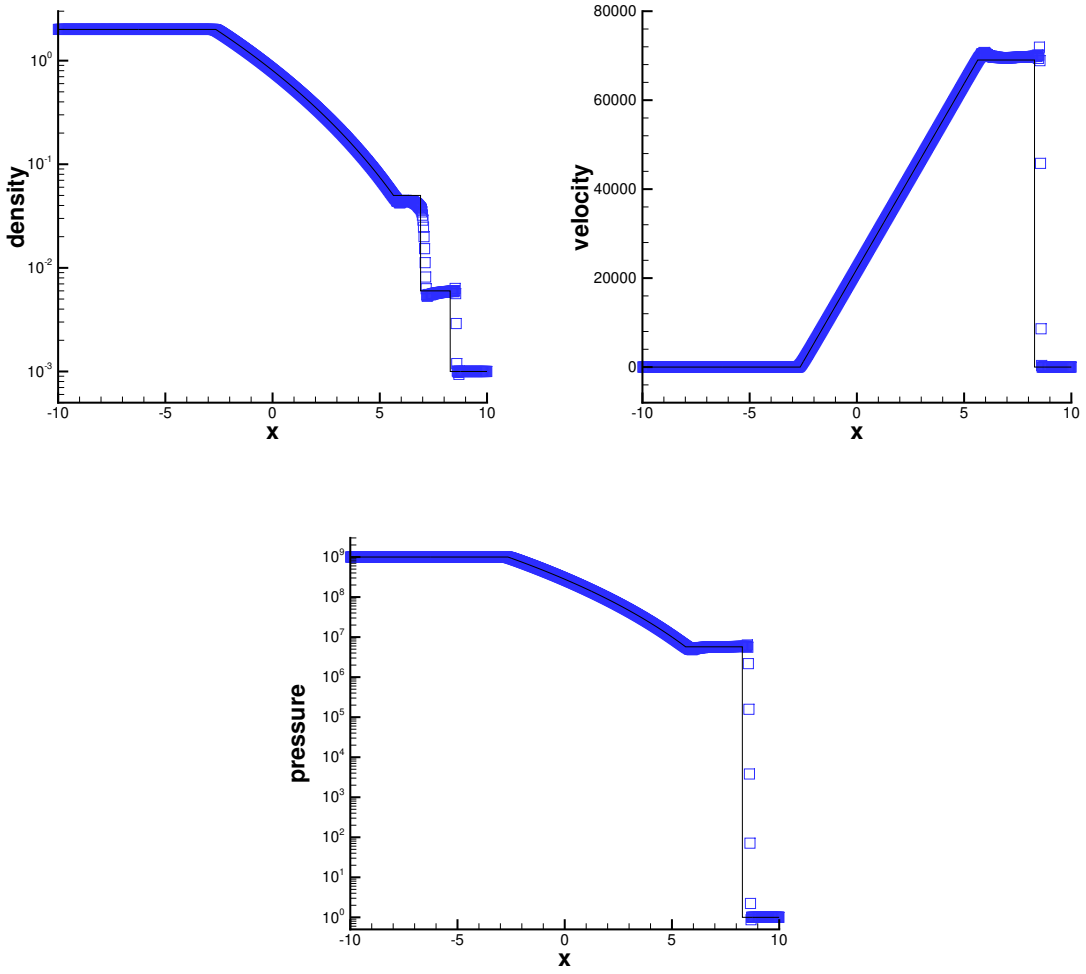

Figure 3: One-dimensional Leblanc problem. $T = 0.0001$ and $N = 800$. Solid line: exact solutions; square: numerical solutions.

Our one-dimensional results are comparable to the results of PP WENO [25, 26] and PP HWENO [2, 7] schemes. Finally, we consider two two-dimensional low density and low pressure problems of (38) for ideal gas.

Example 5.8 (2D Sedov problem). Consider the two-dimensional Sedov blast wave of (38). For the initial condition, the density is 1, velocity is 0, total energy is 10^{-12} everywhere except that the energy in the lower left corner cell is the constant $\frac{0.244816}{\Delta x \Delta y}$. The computational domain is $[0, 1.1] \times [0, 1.1]$ and $\gamma = 1.4$. The reflective boundary condition is applied on the left and bottom edges, and the boundary conditions for the right and top edges are outflow. ε in the nonlinear weights of WENO reconstruction is chosen to be 10^{-20} for this extreme problem. We compute up to $T = 1.0$. In Figure 4, we present the density contour plot and a cut of the density along $x = y$ with a 280×280 mesh.

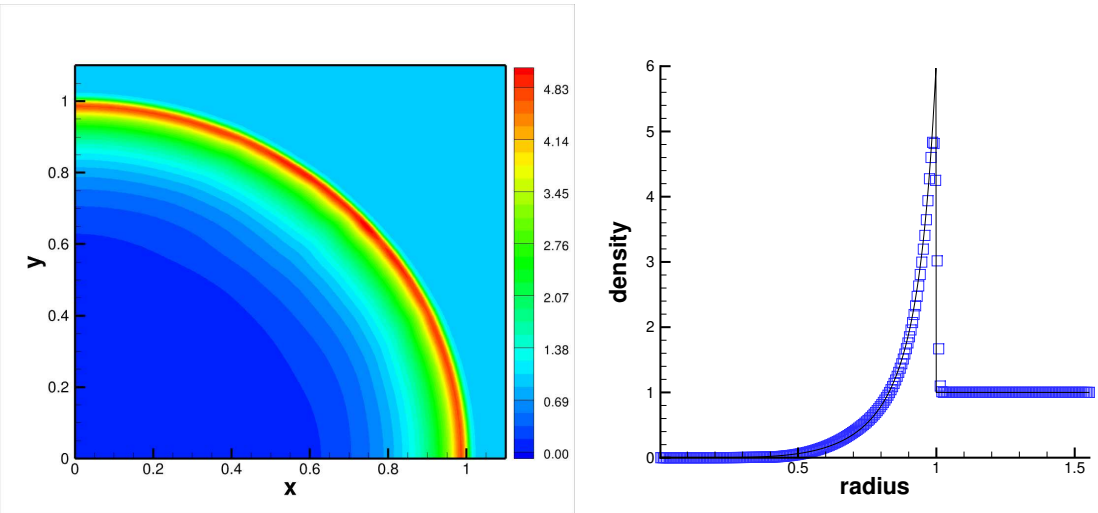

Figure 4: Two-dimensional Sedov problem. $T = 1.0$ and $\Delta x = \Delta y = \frac{1.1}{280}$. Left: 30 equally spaced density contours from 0 to 5; right: cut along $x = y$ for density. Solid line: exact solution; square: numerical solution.

In addition, we also compare the performance of the fifth-order WENO-AO, WENO-MR [28] and WENO-ZQ [27] reconstructions for this problem. The cut of the density along $x = y$ with a 200×200 mesh by the three different WENO reconstructions are shown in Figure 5. We can observe that the results by the WENO-MR and WENO-ZQ are not good and there are many oscillations in the density. The result by the WENO-AO are much better and match the exact solution very well. This is the reason that we use the WENO-AO reconstruction in our method.

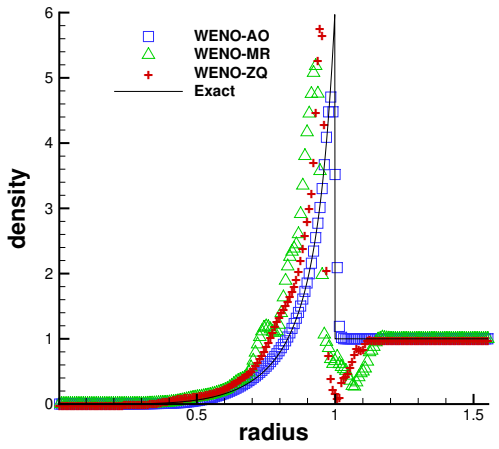

Figure 5: Two-dimensional Sedov problem by different WENO reconstructions. $T = 1.0$ and $\Delta x = \Delta y = \frac{1.1}{200}$. Solid line: exact solution; square: numerical solution by WENO-AO; triangle: numerical solution by WENO-MR; plus: numerical solution by WENO-ZQ.

Example 5.9 (2D shock diffraction problem). Consider the shock diffraction problem of (38). The computational domain is the union of $[0, 1] \times [6, 11]$ and $[1, 13] \times [0, 11]$. The initial condition is a pure right-moving shock of Mach=5.09, initially located at $x = 0.5$ and $6 \leq y \leq 11$, moving into undisturbed air ahead of the shock with a density of 1.4 and pressure of 1. The boundary conditions are inflow at $x = 0, 6 \leq y \leq 11$, outflow at $x = 13, 0 \leq y \leq 11, 1 \leq x \leq 13, y = 0$ and $0 \leq x \leq 13, y = 11$, and reflective at the walls $0 \leq x \leq 1, y = 6$ and $x = 1, 0 \leq y \leq 6$. We compute up to $T = 2.3$ and $\gamma = 1.4$. In Figure 6, we present the density and pressure contour plots on a 832×704 mesh ($\Delta x = \Delta y = \frac{1}{64}$). From the results, we can observe that the low density and low pressure emerge due to the diffraction of high speed shock waves at sharp angles.

Again, our two-dimensional results are comparable to the results of PP WENO [25, 26] and PP HWENO [2, 7] schemes. For the above two examples, the percentage of the cells where PP limiter was activated is less than 0.001%.

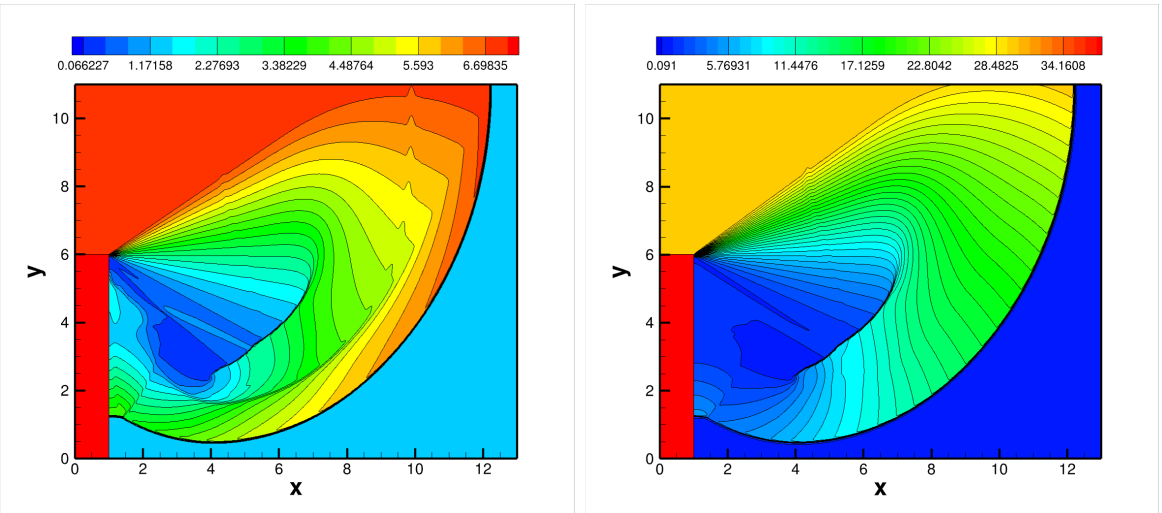

Figure 6: Two-dimensional shock diffraction problem. $T = 2.3$ and $\Delta x = \Delta y = \frac{1}{64}$. Left: 20 equally spaced density contours from 0.066227 to 7.0668; right: 40 equally spaced pressure contours from 0.091 to 37.

6 Concluding remarks

In this paper, we construct maximum-principle-preserving and positivity-preserving central WENO schemes for scalar conservation laws and compressible Euler equations, respectively. The methods are formulated in a finite volume framework on overlapping meshes and require neither numerical fluxes nor flux splitting. In order to keep maximum principle for the solution of scalar conservation laws, or the positivity of the density and pressure in the compressible Euler equations, the general procedures are established for the central WENO schemes with the first-order Euler forward time discretization. High-order SSP Runge-Kutta time discretization will keep such properties. The fifth-order WENO-AO reconstruction [1] outperforms the WENO-MR and WENO-ZQ reconstructions for the 2D Sedov problem. Therefore, the WENO-AO reconstruction is used in our central schemes. The linear weights of the WENO-AO reconstruction can be any positive number provided their sum equals one, and the same nonlinear weights and reconstructed polynomial can be used in different reconstructions (for cell average and point value) which lead to much simpler implementation. Future work includes the design of MPP and PP central WENO schemes with the flux

limiter [22].

Acknowledgment

We would like to thank Dr. Chuan Fan from Southern University of Science and Technology for the helpful discussion.

References

[1] D. S. Balsara, S. Garain, and C.-W. Shu. An efficient class of WENO schemes with adaptive order. *Journal of Computational Physics*, 326:780–804, 2016.

[2] X. Cai, X. Zhang, and J. Qiu. Positivity-preserving high order finite volume HWENO schemes for compressible Euler equations. *Journal of Scientific Computing*, 68(2):464–483, 2016.

[3] G. Capdeville. A central WENO scheme for solving hyperbolic conservation laws on non-uniform meshes. *Journal of Computational Physics*, 227(5):2977–3014, 2008.

[4] Y. Cheng, F. Li, J. Qiu, and L. Xu. Positivity-preserving DG and central DG methods for ideal MHD equations. *Journal of Computational Physics*, 238:255–280, 2013.

[5] A. J. Christlieb, Y. Liu, Q. Tang, and Z. Xu. High order parametrized maximum-principle-preserving and positivity-preserving WENO schemes on unstructured meshes. *Journal of Computational Physics*, 281:334–351, 2015.

[6] B. Einfeldt, C.-D. Munz, P. L. Roe, and B. Sjögreen. On Godunov-type methods near low densities. *Journal of computational physics*, 92(2):273–295, 1991.

[7] C. Fan, X. Zhang, and J. Qiu. Positivity-preserving high order finite volume hybrid Hermite WENO schemes for compressible navier-stokes equations. *Journal of Computational Physics*, 445:110596, 2021.

[8] D. Levy, G. Puppo, and G. Russo. Central WENO schemes for hyperbolic systems of conservation laws. *Esaim Mathematical Modelling and Numerical Analysis*, 33(3):547–571, 1999.

[9] D. Levy, G. Puppo, and G. Russo. Compact central WENO schemes for multidimensional conservation laws. *SIAM Journal on Scientific Computing*, 22(2):656–672, 2000.

[10] D. Levy, G. Puppo, and G. Russo. A fourth-order central WENO scheme for multidimensional hyperbolic systems of conservation laws. *SIAM Journal on Scientific Computing*, 24(2):480–506, 2002.

[11] M. Li, P. Guyenne, F. Li, and L. Xu. A positivity-preserving well-balanced central discontinuous Galerkin method for the nonlinear shallow water equations. *Journal of Scientific Computing*, 71(3):994–1034, 2017.

[12] M. Li, F. Li, Z. Li, and L. Xu. Maximum-principle-satisfying and positivity-preserving high order central discontinuous Galerkin methods for hyperbolic conservation laws. *SIAM Journal on Scientific Computing*, 38(6):A3720–A3740, 2016.

[13] T. Linde and P. L. Roe. Robust euler codes. In *13th Computational Fluid Dynamics Conference*, page 2098, 1997.

[14] Y. Liu. Central schemes on overlapping cells. *Journal of Computational Physics*, 209(1):82–104, 2005.

[15] Y. Liu, C.-W. Shu, E. Tadmor, and M. Zhang. Central discontinuous Galerkin methods on overlapping cells with a nonoscillatory hierarchical reconstruction. *SIAM Journal on Numerical Analysis*, 45(6):2442–2467, 2007.

[16] H. Nessyahu and E. Tadmor. Non-oscillatory central differencing for hyperbolic conservation laws. *Journal of Computational Physics*, 87:408–463, 1990.

[17] J. Qiu and C.-W. Shu. On the construction, comparison, and local characteristic decomposition for high-order central WENO schemes. *Journal of Computational Physics*, 183(1):187–209, 2002.

[18] Z. Tao, F. Li, and J. Qiu. High-order central Hermite WENO schemes on staggered meshes for hyperbolic conservation laws. *Journal of Computational Physics*, 281:148–176, 2015.

[19] Z. Tao, F. Li, and J. Qiu. High-order central Hermite WENO schemes: dimension-by-dimension moment-based reconstructions. *Journal of Computational Physics*, 318:222–251, 2016.

[20] C. Wang, X. Zhang, C.-W. Shu, and J. Ning. Robust high order discontinuous Galerkin schemes for two-dimensional gaseous detonations. *Journal of Computational Physics*, 231(2):653–665, 2012.

[21] T. Xiong, J.-M. Qiu, and Z. Xu. Parametrized positivity preserving flux limiters for the high order finite difference WENO scheme solving compressible Euler equations. *Journal of Scientific Computing*, 67(3):1066–1088, 2016.

[22] Z. Xu. Parametrized maximum principle preserving flux limiters for high order schemes solving hyperbolic conservation laws: one-dimensional scalar problem. *Mathematics of Computation*, 83(289):2213–2238, 2014.

[23] X. Zhang and C.-W. Shu. On maximum-principle-satisfying high order schemes for scalar conservation laws. *Journal of Computational Physics*, 229(9):3091–3120, 2010.

[24] X. Zhang and C.-W. Shu. On positivity-preserving high order discontinuous Galerkin schemes for compressible Euler equations on rectangular meshes. *Journal of Computational Physics*, 229(23):8918–8934, 2010.

[25] X. Zhang and C.-W. Shu. Maximum-principle-satisfying and positivity-preserving high-order schemes for conservation laws: survey and new developments. *Proceedings of the Royal Society A: Mathematical, Physical and Engineering Sciences*, 467(2134):2752–2776, 2011.

[26] X. Zhang and C.-W. Shu. Positivity-preserving high order finite difference WENO schemes for compressible Euler equations. *Journal of Computational Physics*, 231(5):2245–2258, 2012.

[27] J. Zhu and J. Qiu. A new fifth order finite difference WENO scheme for solving hyperbolic conservation laws. *Journal of Computational Physics*, 318:110–121, 2016.

[28] J. Zhu and C.-W. Shu. A new type of multi-resolution WENO schemes with increasingly higher order of accuracy. *Journal of Computational Physics*, 375:659–683, 2018.